NASA TECHNICAL NOTE

NASA TN D-3606

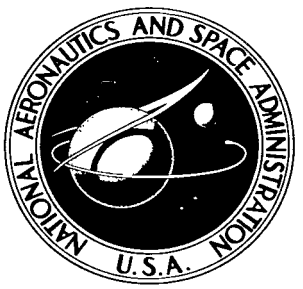

FINITE-THRUST ESCAPE FROM AND CAPTURE INTO CIRCULAR AND ELLIPTIC ORBITS

by Edward A. Willis, Jr.

Lewis Research Center
Cleveland, Ohio

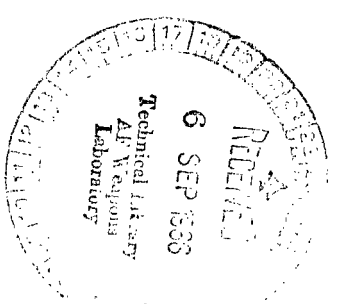

NATIONAL AERONAUTICS AND SPACE ADMINISTRATION • WASHINGTON, D. C. • SEPTEMBER 1966

NASA TN D-3606

FINITE-THRUST ESCAPE FROM AND CAPTURE INTO CIRCULAR AND ELLIPTIC ORBITS

By Edward A. Willis, Jr.

Lewis Research Center
Cleveland, Ohio

NATIONAL AERONAUTICS AND SPACE ADMINISTRATION

For sale by the Clearinghouse for Federal Scientific and Technical Information
Springfield, Virginia 22151 – Price $2.50

FINITE-THRUST ESCAPE FROM AND CAPTURE INTO CIRCULAR AND ELLIPTIC ORBITS

by Edward A. Willis, Jr.

Lewis Research Center

SUMMARY

Finite-thrust escape and capture trajectories are considered which lead from a circular or elliptic orbit to a specified hyperbolic excess velocity vector located at the gravitational "sphere of influence." Each trajectory consists of a powered maneuver initiated at the parking orbit and a coasting arc from the cutoff point to the sphere of influence. The powered maneuver is accomplished with constant, continuous thrust and constant jet velocity. Tangential steering and optimum thrust-initiation points are used to obtain very nearly minimum characteristic velocity increments.

These near-optimal finite-thrust trajectories are analyzed in dimensionless terms and compared with equivalent impulsive ones. The minimal characteristic velocity ratio (that is, the ratio of the actual propulsive effort, $\int a\,dt$, to the equivalent impulsive velocity increment), the optimum characteristic central angle (measured from a reference position on the parking orbit to the asymtotic direction at the sphere of influence), and the optimum initial true anomaly for departing from an elliptic orbit are found for a wide range of planetocentric trajectories. These results are presented as functions of the dimensionless hyperbolic velocity, acceleration, and jet velocity parameters. The dimensionless arguments may be easily scaled to any particular case of interest - for example, a specific planet, parking orbit, propulsion system, and hyperbolic velocity. The data ranges were chosen primarily to correspond with high- to medium-thrust systems, such as chemical rockets and various types of nuclear rockets. These results may be conveniently used in combination with ballistic interplanetary trajectory calculations to obtain a realistic geometric description and accurate propellant fractions for a great variety of interesting and potentially important space flight missions. Examples illustrating the use of these data for actual mission problems are also presented.

INTRODUCTION

The dynamic and geometric effects of finite vehicle acceleration must be accounted for in order to derive accurate propellant fractions (and hence vehicle weight) from ballistic interplanetary trajectory data (such as refs. 1 to 3). The velocity increments obtainable from impulsive calculations are useful in preliminary studies but do not always lead to accurate propellant fractions for vehicles with realistic thrust levels. This is because of the following:

(1) A reduction in propulsive efficiency (also called a "gravity loss") occurs when an impulse is replaced by a finite-thrust maneuver. As a result, the characteristic propulsive velocity increment (ΔV_{ch}) and propellant fraction increase.

(2) There is often a considerable difference between the geometric properties of impulsive and finite-thrust trajectories. This, in turn, may complicate the problem of matching heliocentric and planetocentric trajectory segments.

The efficiency penalty due to finite thrust may be accounted for by applying a correction factor (also termed characteristic velocity ratio) to the impulsive velocity increment. Accurate propellant fractions may then be obtained in a convenient and familiar way from the classical rocket equation. Prior discussions of this approach (e.g., refs. 4 and 5) presented some typical velocity correction factors, but no geometric data, and considered only circular parking orbits and escape maneuvers. An alternative approach (ref. 6) is to present the propellant fraction directly. In principle, this is equivalent to the correction factor approach but is less convenient to use because a greater amount of interpolation is required. A considerable amount of data of this nature is given in reference 6, which is limited, however, to the case of circular orbits. The present report includes a wide range of velocity correction factors and geometric data for both escape and capture maneuvers and for elliptic as well as circular initial orbits. This report is intended both as a generalization of references 4 and 5 and to complement available and future ballistic trajectory data. The correction factors and geometric data presented herein may be used together with ballistic interplanetary data to obtain accurate propellant fractions and realistic overall geometry for many missions of practical interest.

Trajectories that use a single burning period followed by coasting to the sphere of influence are analyzed herein. The powered maneuver begins at an optimum point on the initial orbit and proceeds with constant thrust and constant jet velocity until the hyperbolic excess velocity attains a prescribed magnitude. After cutoff, the vehicle continues along a Keplerian arc to the sphere of influence. The final asymptotic direction of the hyperbolic excess velocity vector is left open. For such trajectories, it is shown that tangential steering yields very nearly the minimum characteristic velocities and propellant fractions.

Characteristic velocity ratios, optimum initial true anomalies, and final asymptotic

directions are derived from a study of these unconstrained trajectories. The results are presented as functions of the initial orbit elements and the dimensionless hyperbolic velocity, jet velocity, and acceleration parameters. The significance of each dimensionless variable is discussed, and scaling rules are developed to apply the generalized data to any specific case of interest. As a sample application, the scaling procedures are used to generate a set of specific working data curves that describe typical nuclear rocket maneuvers near Venus, Earth, and Mars. Further examples illustrate the use of the present results in solving representative mission analysis problems such as the selection of an advantageous parking orbit radius and optimization of the initial thrust to weight ratio.

SYMBOLS

A acceleration

a dimensionless acceleration

e eccentricity of conic section

F thrust

f_v characteristic velocity ratio or correction factor, $\Delta V_{ch}/\Delta V_{imp}$

G acceleration due to gravity

g dimensionless acceleration due to gravity

H angular momentum

h dimensionless angular momentum

$\mathcal{H}$ auxiliary function, defined in equation (A1)

I specific impulse, sec

k structural mass fraction, see equation (43)

M mass

m mass fraction

P semilatus rectum

p dimensionless semilatus rectum

R polar radius

r radius ratio

t time

u	angle of attack
V	velocity
v	dimensionless velocity
ΔV	velocity increment
Δv	dimensionless velocity increment
α	trajectory path angle
η	efficiency
θ	trajectory central angle
θ_{ch}	characteristic central angle
μ	planet gravitational constant
ν	parking orbit true anomaly at thrust initiation (escape maneuver) or at thrust termination (capture)
τ	dimensionless time
ψ	adjoint variables, defined in equation (A2)
$( )'$	denotes differentation with respect to τ
$\langle \rangle$	denotes mean value

Subscripts:

act	actual
as	acceleration sensitive
bo	burnout
c	circular
cap	capture
ch	characteristic
cst	coasting
esc	escape
g	gross
i	initial
imp	impulsive
j	jet

k, n	general numerical indices
ℓ	payload
m	mean
max	maximum
min	minimum
opt	optimum
p	propellant
pl	planet
po	parking orbit
pr	propulsive
ps	propellant sensitive
pwr	powered
ref	reference
sc	spacecraft
ts	thrust sensitive
∞	sphere of influence
$\oplus$	Earth
♀	Venus
♂	Mars

ANALYSIS

The initial mass of a space vehicle M_i is a useful criterion for interplanetary mission studies. A major step in computing M_i is to determine the propellant fraction m_p for each propulsive maneuver. The propellant fractions are derived in turn from a study of the flight trajectory, which is illustrated in typical form in figure 1(a). The flight path consists of alternate planetocentric arcs (view A) and heliocentric arcs (view B), which are matched at the spheres of influence as indicated in view A; that is,

$$\vec{V}_{\infty,\,\text{planetocentric trajectory}} = \left(\vec{V}_{sc} - \vec{V}_{pl}\right)_{\text{heliocentric trajectory}} \tag{1}$$

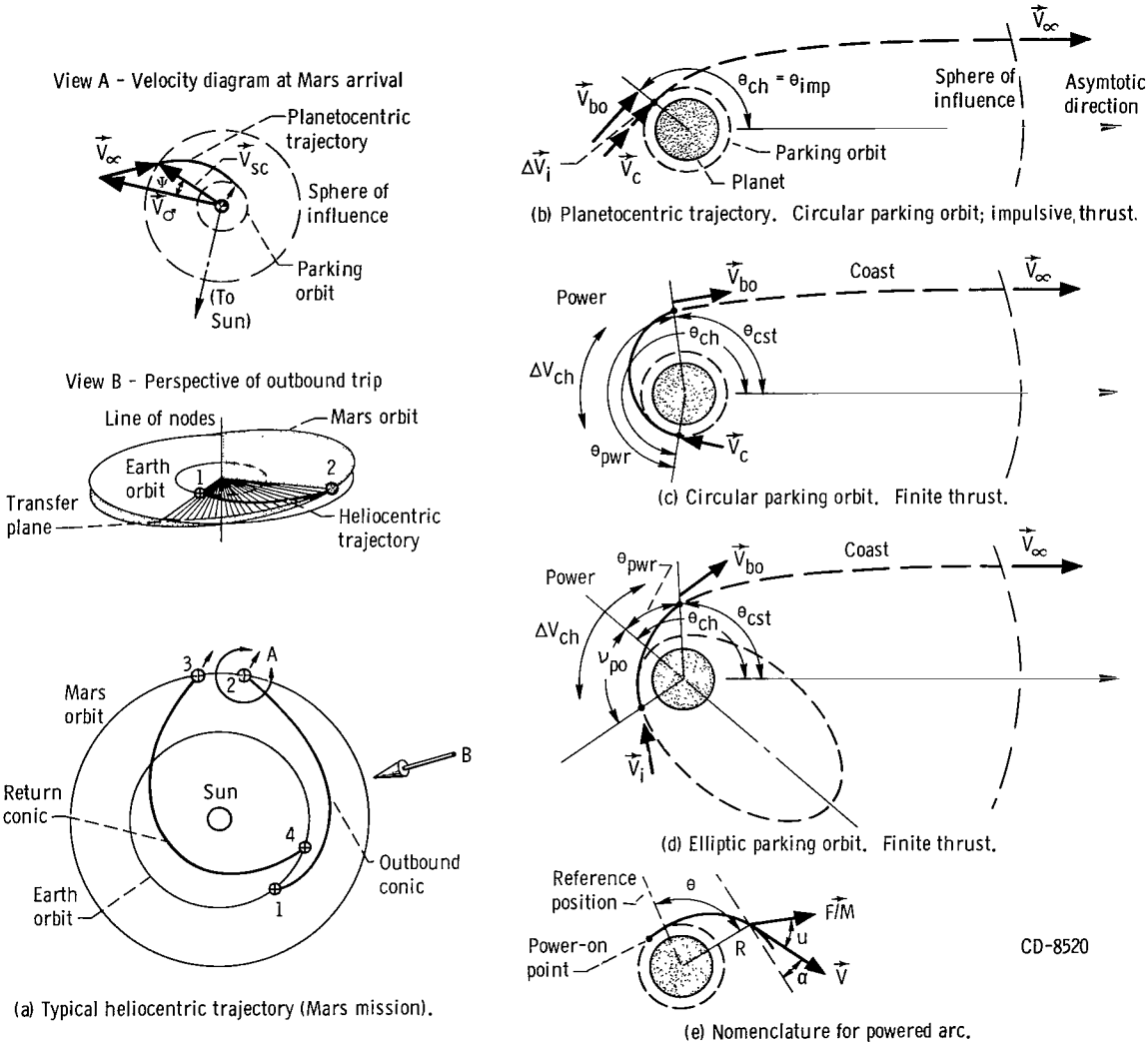

Figure 1. - Elements of patched conic trajectories.

Either type of arc may contain a propulsive maneuver. For all but very low-thrust systems, the propulsive effort or ΔV_{ch} of a heliocentric maneuver (used as a midcourse correction or, as in ref. 3, to reduce the total ΔV) may be determined accurately by impulsive methods. Values of m_p are then given by the familiar formula

$$m_p = 1 - \exp\left(\frac{-\Delta V_{imp}}{V_j}\right) \tag{2}$$

Planetocentric trajectories (illustrated in figs. 1(b) to 1(d)) join a parking orbit and must produce a "hyperbolic excess velocity" vector $\vec{V}_\infty$ (as defined by eq. (1)) at the sphere of influence. Relative to the parking orbit, $\vec{V}_\infty$ is represented by its magnitude V_∞ and direction θ_{ch}. These two parameters together with the parking orbit elements define boundary conditions for each end of the planetocentric trajectory. Impulsive maneuvers to satisfy these boundary conditions (fig. 1(b)) can be easily computed, but they often lead to erroneous values of m_p. The effects of finite thrust and other neglected items can be lumped into a "correction factor" f_v, which will be so defined that accurate propellant fractions for finite-thrust maneuvers (figs. 1(c) and 1(d)) can still be obtained from an expression of the same simple form as equation (2); that is,

$$m_p = 1 - \exp\left(\frac{f_v \Delta V_{imp}}{V_j}\right) \tag{3}$$

The quantity $f_v \Delta V_{imp}$ may be recognized as the actual propulsive effort or characteristic velocity ΔV_{ch} for the finite-thrust maneuver. Thus f_v is defined, for computational purposes, as

$$f_v = \frac{\Delta V_{ch}}{\Delta V_{imp}} = \frac{1}{\Delta V_{imp}} \int_0^{t_{bo}} \frac{\text{Thrust}}{\text{Mass}}\, dt \tag{4}$$

and is termed the characteristic velocity ratio.

It is convenient to define ΔV_{imp} as the minimum ΔV which will produce the same magnitude of V_∞ from the same parking orbit as does the finite-thrust maneuver (without regard to the value of θ_{ch}). As is well known, the control policy that minimizes ΔV_{imp} is to apply the impulse tangent to the parking orbit and at periapse if the orbit is elliptic. With this definition, ΔV_{imp} can be easily computed in closed form. Since

ΔV_{imp} is minimal, $f_v \geq 1$ (it will be shown later that f_v is also bounded below 3.0 in the case of circular orbits).

On the other hand, ΔV_{ch} is obtained by numerical integration, thus accounting for finite thrust and jet velocity, possible geometric constraints on θ_{ch}, and actual (as opposed to optimal) control policies in addition to V_∞ and the parking orbit elements. Consequently, f_v reflects these same factors.

For impulsive trajectories, the characteristic angle consists only of a coasting arc θ_{imp} as figure 1(b) illustrates. When finite thrust is used, θ_{ch} consists of a powered central angle θ_{pwr} plus a coasting arc θ_{cst} as indicated in figure 1(c). The sum of these two contributions is generally larger than the coasting angle θ_{imp}, which corresponds to an impulsive trajectory. Thus, the power-on point must be advanced in the finite-thrust case in order to attain a prescribed direction of $\vec{V}_\infty$ in inertial space.

The quantities f_v and θ_{ch} define the essential properties of finite-thrust trajectories that begin or end in circular or elliptic orbits. The values of m_p obtainable from precomputed f_v data by means of equation (3) are more accurate than those which could be obtained if m_p were plotted directly (as in ref. 6). This is because ΔV_{imp} is always maintained as the first approximation to ΔV_{ch}. For the same reason, the present approach is often more convenient to use; in many cases, constant "typical" values of f_v can be chosen that will yield acceptably accurate values of m_p without laborious interpolation.

Assumptions

The following assumptions have been introduced in order to simplify the numerical calculations:

(1) As previously mentioned, an overall trajectory consists of successive two-body arcs joined at the planet's gravitational sphere of influence.

(2) Each arc lies in a plane determined by $\vec{V}_\infty$ and the center of force, and the gravitational attraction along each arc is represented by an inverse square central force field.

(3) The propulsion system operates with constant continuous thrust and constant jet velocity. The thrust is considered finite, but large enough that the necessary magnitudes of $\vec{V}_\infty$ can be attained within the sphere of influence. The radius of the sphere of influence is assumed to be much larger than that of the initial planetocentric orbit.

(4) The sphere of influence boundary condition is taken to be the magnitude $|\vec{V}_\infty|$ only. The characteristic angle θ_{ch}, which defines the orientation of the initial orbit relative to $\vec{V}_\infty$, is not constrained but is treated as a dependent variable. Therefore, for given V_∞ and parking orbit elements, the factors that primarily affect θ_{ch}, namely the

power-on or -off point ν_{po} (cf fig. 1(d)) and the steering control policy u(t) (i.e., the angle of attack program), can be chosen solely to minimize ΔV_{ch} and hence f_v. Trajectories of this kind will be termed "optimum-angle" trajectories herein. Such trajectories can always be used with a circular orbit since any necessary direction of $\vec{V}_\infty$ in inertial space can be attained, without changing f_v, by selecting the appropriate power-on or -off point. The optimum angle can also be used for one maneuver based on a given elliptic orbit. If an elliptic orbit is used at the destination planet of a round-trip mission, it must be reoriented between arrival and departure in order to use optimum-angle trajectories for both capture and escape. Several effective methods of reorienting an elliptic orbit are described in references 7 and 8; these methods would permit optimum-angle trajectories to be used for both escape and capture maneuvers.

(5) Tangential steering (i.e., zero angle of attack) is used to approximate the optimal steering policy. If θ_{ch} is not constrained, tangential steering yields the minimum propulsive effort in the limit of impulsive thrust. In reference 9 it was shown that, with θ_{ch} not constrained, the penalty for using tangential rather than variational steering for constant acceleration escapes to parabolic energy $\left(V_\infty^2 = 0\right)$ from a circular orbit is quite small (under 1 percent) regardless of the mangitude of the acceleration. In appendix A, the analysis of reference 9 is generalized to include constant thrust, constant jet velocity, hyperbolic burnout energy ($V_\infty > 0$), and elliptic as well as circular orbits. It is shown that the maximum penalty for tangential steering is still under 1 percent of ΔV_{ch} under these more general conditions, and it decreases rapidly as elliptic orbits of increasing eccentricity are considered.

Equations of Motion

When the foregoing assumptions are used, a simple set of differential equations may be constructed to describe the rocket's motion.

Coordinate system and dimensionless variables. - The trajectory is represented in plane polar coordinates as indicated in figures 1(b) to 1(e). The position of the rocket $\vec{R}$ is described by the polar radius R and central angle θ (fig. 1(e)); the velocity $\vec{V}$ is denoted by its magnitude V and path angle α relative to the local horizontal. Similarly, the acceleration $\vec{A}$ is described by its magnitude F/M and angle of attack u (relative to $\vec{V}$). Gravity $\vec{G}$ is represented by its magnitude μ/R^2 and is directed toward the center of force.

In order to obtain general results, it is necessary to normalize the variables just described. The resulting dimensionless variables (denoted by lower case symbols) are obtained by dividing radii, velocities, accelerations, and time, respectively, by the radius, circular velocity, local gravity, and circular radian period corresponding to a

reference position on the initial orbit. Polar angles (θ) are also measured relative to the reference position. For circular orbits, the reference position is the power-on or -off point, but for elliptic orbits the periapse is the reference point. The dimensionless variables, which will be used henceforth, are related to their dimensional counterparts by

$$r(\tau) = \frac{R(t)}{R_{ref}} \tag{5a}$$

$$v(\tau) = \frac{V(t)}{V_{c,\,ref}} \tag{5b}$$

$$a(\tau) = \frac{A(t)}{\mu/R_{ref}^2} \tag{5c}$$

$$\tau = \frac{V_{c,\,ref}}{R_{ref}}\, t \tag{5d}$$

$$g = \frac{G}{\mu/R_{ref}^2} = \frac{1}{r^2} \tag{5e}$$

$$v_j = \frac{G_{\oplus} I}{V_{c,\,ref}} \tag{5f}$$

$$v_{\infty}^2 = \left(\frac{V_{\infty}}{V_{c,\,ref}}\right)^2 \tag{5g}$$

Basic equations. - With the normalization just described, the first-order vector equations of motion are

$$\vec{r}\,' = \vec{v} \tag{6a}$$

$$\vec{v}\,' = \vec{a} + \vec{g} \tag{6b}$$

The components of equation (6) for r, v, α, and θ are then

$$r' = v \sin \alpha \tag{7a}$$

$$v' = a \cos u - \frac{\sin \alpha}{r^2} \tag{7b}$$

$$\alpha' = \frac{a \sin u}{v} + \left(v^2 - \frac{1}{r}\right) \frac{\cos \alpha}{rv} \tag{7c}$$

$$\theta' = \frac{v}{r} \cos \alpha \tag{7d}$$

The characteristic velocity ΔV_{ch} which is needed to define f_v is given by

$$\Delta V'_{ch} = a(\tau) \tag{8}$$

Since the vehicle operates with constant thrust and jet velocity, the acceleration $a(\tau)$ is given, for an escape maneuver, by

$$a(\tau)_{esc} = \frac{a_{po}}{1 - a_{po}\tau/v_j} \qquad 0 \leq \tau \leq \tau_{bo}$$

$$= 0 \qquad \tau_{bo} < \tau \text{ (coasting flight)} \tag{9a}$$

where $a_{po} = a_i$, the initial acceleration at the power-on point.

Capture maneuvers, on the other hand, are integrated backward in time, that is, beginning at the desired power-off point on the orbit. This is done only for computational convenience (to avoid the iterative search that would otherwise be required) but has the consequence that the acceleration term for capture maneuvers is given by

$$a(\tau)_{cap} = \frac{a_{po}}{1 + a_{po}\tau/v_j} \qquad 0 \leq \tau \leq \tau_{bo}$$

$$= 0 \qquad \tau_{bo} < \tau \text{ (coasting flight)} \tag{9b}$$

In this case a_{po} is to be interpreted as the acceleration at burnout rather than the initial one. For either escape or capture maneuvers, the initial and burnout accelerations are related by

$$a_{bo} = \frac{a_i}{1 - m_p} = \frac{a_i}{1 - \dfrac{a_i \tau_{bo}}{v_j}} \tag{10a}$$

or

$$a_i = \frac{a_{bo}}{1 + \dfrac{a_{bo}\tau_{bo}}{v_j}} = \frac{a_{bo}}{1 + \dfrac{M_p}{M_{bo}}} \tag{10b}$$

Boundary conditions. - In terms of the present dimensionless variables, the initial ($\tau = 0$) conditions for a circular orbit are

$$r(0) = 1 \tag{11a}$$

$$v(0) = 1 \tag{11b}$$

$$\alpha(0) = 0 \tag{11c}$$

$$\theta(0) = 0 \tag{11d}$$

For an elliptic parking orbit, the initial conditions are given in terms of the eccentricity of the orbit e_{po} and the true anomaly of the power-on or -off point ν_{po} by the well-known conic equations

$$r(0) = \frac{1 + e_{po}}{1 + e_{po} \cos \theta(0)} \tag{12a}$$

$$v(0) = \left[\frac{2}{r(0)} - (1 - e_{po})\right]^{1/2} \tag{12b}$$

$$\alpha(0) = \tan^{-1}\left[\frac{e_{po} r(0) \sin \theta(0)}{1 + e_{po}}\right] \tag{12c}$$

$$\theta(0) = \nu_{po} \tag{12d}$$

With these initial conditions and a known form for the steering control law (for example, $u(\tau) \equiv 0$), the equation of motion may be integrated (numerically) to obtain r, v, α, and θ as functions of τ with ν_{po}, e_{po}, v_∞, a_{po}, and v_j as parameters. Thrust is terminated at the burnout time τ_{bo}, at which time the desired energy or hyperbolic velocity has been attained (cf eq. (1)), that is, when

$$v_\infty^2(\tau_{bo}) = v^2(\tau_{bo}) - \frac{2}{r(\tau_{bo})} = v_\infty^2 \Bigg|_{\text{at sphere of influence}} = \frac{|\vec{v}_{sc} - \vec{v}_{pl}|^2}{v_{c,ref}^2} \tag{13}$$

Once τ_{bo} has been determined, equations (8) and (9) may be evaluated as a definite integral; that is,

$$\Delta v_{ch}(\tau_{bo}) \triangleq \int_0^{\tau_{bo}} a(\tau)d\tau = v_j \ln\left(\frac{1}{1 - \frac{a_i \tau_{bo}}{v_j}}\right) \tag{14}$$

The properties of the remainder of the trajectory, that is, the coast from burnout to the sphere of influence, may finally be calculated in closed form from the well-known conic equations.

Trajectory Solutions

There are no known general closed-form solutions to the equation of motion described above. As has been previously mentioned, accurate values of Δv_{ch}, θ_{ch}, and other trajectory parameters can only be obtained by numerical integration. Impulsive solutions, which can be obtained in closed form, are required to define values of Δv_{imp} and thus of f_v. Low-thrust limiting solutions are also studied to derive an upper bound for f_v and to obtain insight into the behavior and significance of this function.

Impulsive thrust. - For tangential steering ($u(\tau) = 0$), only the velocity equation (7b) contains a. For sufficiently high thrust, and/or for very low local gravity, the dimensionless acceleration a tends toward infinity during the powered maneuver, but the duration of the maneuver τ_{bo} tends toward zero. In the impulsive limit, v changes discontinuously across the maneuver, but r, α, and θ remain constant. The velocity equation (7b) can then be integrated in closed form to yield the "classical rocket equation" (2). The appropriate value of $\Delta v_{imp} (= v_{bo} - v_i)$ may then be derived from equa-

tions (12b) and (13) when it is recalled that the impulse is not only tangential but is to be applied at the periapse if the orbit is elliptic; that is,

$$\Delta v_{imp} = \left(v_\infty^2 + 2\right)^{1/2} - \left(1 + e_{po}\right)^{1/2} \tag{15}$$

This is the value which enters the definition of f_v (eq. (4)).

The remainder of the planetocentric trajectory consists of a coasting arc (i.e., a hyperbola) whose periapse is at the impulse point and whose asymtotic branch extends to the sphere of influence (recall fig. 1(b)). Since the sphere of influence is considered very large compared to the parking orbit, the characteristic angle θ_{ch} is well approximated by the asymtotic true anomaly of the hyperbola; that is,

$$\theta_{ch,\,imp} = \cos^{-1}\left(-\frac{1}{e_{bo}}\right) = \theta_{cst} \tag{16}$$

where

$$e_{bo} = v_\infty^2 + 1 \tag{17}$$

Finite thrust. - The powered portion of the trajectory is integrated numerically to obtain values of r, v, α, and θ at the burnout time τ_{bo}, in addition to a value of ΔV_{ch} for use in equation (4). The remainder of the trajectory, that is, the coast from the burnout point to the sphere of influence, is again a conic arc whose elements may be computed in terms of the burnout conditions r_{bo}, v_{bo}, α_{bo}, and θ_{bo}. The semilatus rectum p_{bo} is given by

$$p_{bo} = r_{bo}^2 v_{bo}^2 \cos^2 \alpha_{bo} \tag{18a}$$

and the eccentricity e_{bo} by

$$e_{bo} = \left(1 + p_{bo} v_\infty^2\right)^{1/2} \tag{18b}$$

Then the coasting contribution (θ_{cst}) may be computed from the conic equation and added to θ_{bo} to obtain

$$\theta_{ch} = \theta_{bo} + \cos^{-1}\left(-\frac{1}{e_{bo}}\right) - \cos^{-1}\left(\frac{p_{bo}/r_{bo} - 1}{e_{bo}}\right) \tag{19}$$

Very low thrust. - A useful approximate solution may be obtained in closed form for maneuvers with very low but finite thrust. It is assumed that

$$a(\tau) << \frac{1}{r^2}(\tau) \qquad v_\infty^2 \leq 0 \tag{20a}$$

but that

$$a(\tau) >> \frac{1}{r^2}(\tau) \qquad v_\infty^2 > 0 \tag{20b}$$

That is, escape $\left(v_\infty^2 = 0\right)$ is attained at a very great radius, and further energy is then added in a field-free region. If the initial orbit is circular it will remain nearly circular, that is, a spiral of low pitch. This means that α is small and moreover that $\alpha' \approx 0$. Equation (7c) then yields, for tangential steering, the condition

$$v^2 \approx \frac{1}{r} \tag{21}$$

Combining this relation with equations (7a) and (7b) yields

$$(\Delta v_{ch})' = v' + \frac{r'}{r^{3/2}} \tag{22a}$$

or

$$d(\Delta v_{ch}) = dv + d\left(\frac{2}{\sqrt{r}}\right) \tag{22b}$$

Integrating term by term and applying initial condition (11) and the terminal conditions

$$\left.\begin{aligned} r(\tau_{bo}) &\to \infty \\ v(\tau_{bo}) &\to v_\infty \end{aligned}\right\} \tag{23}$$

yield the result that

$$\Delta v_{ch,\ \text{very low thrust, circular orbit}} \approx v_\infty - v_i + \frac{2}{\sqrt{r_i}} - \frac{2}{\sqrt{r_{bo}}} = v_\infty + 1 \tag{24}$$

so that

$$f_{v,\ \text{very low thrust, circular orbit}} \approx \frac{v_\infty + 1}{\left(v_\infty^2 + 2\right)^{1/2} - 1} \tag{25}$$

It will be shown in the next section that Δv_{ch} is directly proportional to the change in v_∞^2 that occurs in going from the initial orbit to the burnout point; that is, $\Delta v_{ch} \propto \left(v_{\infty,bo}^2 - v_{\infty,po}^2\right)$. This suggests that Δv_{ch} for an elliptic orbit departure should be approximately the same as for a departure from a circular orbit whose energy is equal to the energy of the ellipse. Since

$$v_{\infty,\ \text{elliptic po}}^2 = e_{po} - 1 = v_{\infty,\ \text{equivalent circular po}}^2 = \frac{-1}{r_{c,\ \text{equivalent}}} \tag{26}$$

the radius of this equal-energy circular orbit is

$$r_{c,\ \text{equivalent}} = \frac{1}{1 - e_{po}} \tag{27}$$

If (27) is used in place of (11a), equation (24) becomes

$$\Delta V_{ch,\ \text{ellipse, low thrust}} = v_{\infty,bo} + (1 - e_{po})^{1/2} \tag{28}$$

and the corresponding value of f_v is

$$f_{v,\ \text{very low thrust, elliptic po}} \approx \frac{v_{\infty,bo} + (1 - e_{po})^{1/2}}{\left(v_{\infty,bo}^2 + 2\right)^{1/2} - (1 + e_{po})^{1/2}} \tag{29}$$

It may be seen by inspection of equation (25) that f_v for a circular orbit has a maxi-

mum value of 3 where $v_\infty = 0.5$. This is the desired upper bound. For elliptic orbits, it may be seen from (29) that the upper bound is an increasing function of e_{po}. If $e_{po} = 0.9$, for instance, the maximum value of f_v is about 10.6 (rather than 3) and occurs when $v_\infty \approx 0.15$. It will be demonstrated in the RESULTS that equations (25) and (29) not only yield valid upper bounds for f_v but also provide an accurate qualitative description of how f_v varies with v_∞^2 for low-thrust systems.

Mean value solutions. - A formal solution for Δv_{ch} useful in interpreting the behavior and significance of f_v may be derived by converting the velocity equation (7b) into an energy equation. Multiplying by v and using equation (7a) yield

$$v v' + \frac{r'}{r^2} = va \cos u \tag{30a}$$

or (recalling eq. (13)),

$$\frac{1}{2}\left(v_\infty^2\right)' = a(v \cos u) \tag{30b}$$

This may be formally integrated, using the law of the mean, to obtain the symbolic result

$$\Delta v_{ch} = \frac{v_{\infty,bo}^2 - v_{\infty,po}^2}{2\langle v \cos u \rangle} \tag{31}$$

where $\langle v \cos u \rangle$ is the mean tangential velocity obtained by averaging $v \cos u$ with respect to Δv_{ch}. When the same argument is applied to an impulsive trajectory, it is seen that

$$f_v \triangleq \frac{\Delta v_{ch}}{\Delta v_{imp}} = \frac{\langle v \cos u \rangle_{imp}}{\langle v \cos u \rangle_{actual}} \tag{32a}$$

That is, f_v may be expressed as the ratio of the mean tangential velocity for an impulsive maneuver to that of the actual finite-thrust maneuver. In principle, f_v may be determined by comparing the velocity and steering histories of actual and impulsive maneuvers. (Examples of this will be given in the DISCUSSION.) For a given value of Δv_∞^2, the parameters a_{po}, v_j, and ν_{po} only affect f_v by their influence on v.

On the other hand, the steering control $u(\tau)$ enters f_v explicitly, as is clearly shown in (31) or (32a). It is evident that tangential steering ($u(\tau) \equiv 0$) will produce the

maximum instantaneous value of v cos u. Improvements in the mean value $\langle v \cos u \rangle$ by means of variational steering can only come about by increasing v at the expense of cos u. These opposing trends explain the fact, demonstrated in appendix A, that there is little to be gained by using variational rather than tangential steering for optimum-angle trajectories. If tangential steering is used, (32a) becomes

$$f_v = \frac{\langle v \rangle_{imp}}{\langle v \rangle_{actual}} \tag{32b}$$

Thus, the selection of the power-on point ν_{po} to minimize f_v is in accordance with the intuitive principle that energy can be added most efficiently in a region of high velocity. In fact, it is easy to see that f_v is a direct measure of the mean propulsive efficiency defined by

$$\eta_{pr,\,m} = \frac{\frac{1}{2} M_{bo} \Delta v_\infty^2}{\frac{1}{2} M_p v_j^2} \triangleq \frac{\text{Energy added to final mass}}{\text{Useful energy liberated by propulsion system}} \tag{33}$$

Then, the ratio of $\eta_{pr,\,m}$ for an actual maneuver to that for the equivalent impulsive manuever is (assuming equal M_{bo})

$$\frac{(\eta_{pr,\,m})_{actual}}{(\eta_{pr,\,m})_{imp}} = \frac{M_{p,\,imp}}{M_{p,\,actual}} \triangleq \frac{1}{f_p} \tag{34}$$

If equations (2) and (3) are used for M_p, $1/f_p$ may be expressed as

$$\frac{1}{f_p} = \frac{\exp(f_v \, \Delta v_{imp}/v_j) - 1}{\exp(\Delta v_{imp}/v_j) - 1}$$

$$= f_v \left\{ 1 + \frac{f_v - 1}{2} \left(\frac{\Delta v_{imp}}{v_j} \right) \left[1 + \frac{2f_v - 3}{6} \left(\frac{\Delta v_{imp}}{v_j} \right) \cdots \right] \right\} \tag{35}$$

Therefore,

$$f_v \approx \frac{1}{f_p} = \frac{(\eta_{pr,m})_{imp}}{(\eta_{pr,m})_{actual}} \tag{36}$$

to the first order in $(\Delta v_{imp}/v_j)$. Thus, f_v varies inversely with the mean propulsive efficiency.

f_v as a "gravity loss". - It is evident from equation (31) that f_v contains both dynamic effects (i.e., Δv_∞^2) and geometric effects ($\langle v \cos u \rangle$), neither of which depends explicitly on the presence or absence of a gravitational field. In the general case, f_v can represent "steering losses" as much as gravity losses. For the optimum-angle trajectories which are of primary interest, however, there are no steering losses as such; therefore, f_v may be interpreted as a gravity loss in the sense that it accounts for dynamic phenomena (reduction of $\langle v \rangle$ and $\eta_{pr,m}$) that are caused in turn by the gravity field. As here defined and used, however, f_v cannot be directly related to a kinematic gravity loss of the form

$$\Delta v_{gravity\ loss} = \int_0^{\tau_{bo}} \frac{\sin \alpha}{r^2} d\tau \tag{37}$$

When tangential steering is assumed in (7b), it may be seen that

$$\Delta v_{gravity\ loss} = \Delta v_{ch} - \Delta v \tag{38}$$

while the loss associated with f_v is

$$\Delta v_{loss,\, f_v} = \Delta v_{imp}(f_v - 1) = \Delta v_{ch} - \Delta v_{imp} \tag{39}$$

A definition of f_v based on equation (37) would not necessarily represent a loss of energy since it would apply to coasting (constant energy) orbits as well as to powered maneuvers. Furthermore, such an interpretation cannot be used to explain the fact that, in the low-thrust limit, f_v continues to increase beyond $v_\infty = 0$. At this point ($r \to \infty$) all of the gravity field has been left behind, but as may be seen from equation (25), f_v increases from 2.414 to 3.000 as v_∞ increases from 0 to 0.5. It will be shown in the DISCUSSION that this typical behavior can be adequately explained in terms of $\langle v \rangle$.

RESULTS

The equations of motion and auxiliary formulae indicated in the preceding section were programed for numerical integration on a high-speed digital computer. Values of f_v and θ_{ch} were then obtained which correspond to a wide range of propulsive maneuvers.

Dimensionless Data

The quantities f_v and θ_{ch}, which describe the overall dynamic and geometric characteristics of optimum-geometry trajectories, are plotted against the dimensionless hyperbolic velocity parameter v_∞^2. Both escape and capture maneuvers are considered over a range of values of the dimensionless variables a_{po} and v_j.

Results pertaining to maneuvers leading from or to a circular orbit are presented in figure 2. The dependent variable (i.e., f_v or θ_{ch}) and the range of dimensionless agruments covered by the figure are listed in table I. It has been previously noted that any desired orientation of $\vec{v}_\infty$ inertial space can be attained without changing f_v simply by selecting the appropriate thrust-initiation point on the ciruclar orbit. Consequently, the value of θ_{ch} is of little concern for circular orbits and θ_{ch} data are presented for only two cases - figures 2(b) and 2(i).

As indicated in table II (p. 29), the corresponding results for elliptic orbits (with $e_{po} = 0.9$) are presented in figure 3. In this case, θ_{ch} defines the required orientation of the ellipse with respect to $\vec{v}_\infty$. It may be recalled by again referring to figure 1(d) that reference conditions for an elliptic orbit are defined by the periapse radius vector. The characteristic central angle θ_{ch} is measured from periapse regardless of the initial power-on point (ν_{po}). The reference impulsive Δv (eq. (3)) used in defining f_v is computed at periapse even if the actual trajectory begins at some other position ($\nu_{po} \neq 0$) on the ellipse.

Conversion of Dimensionless Data to Dimensional Form

The preceding dimensionless results can be applied in any case of physical interest. That is, the reference values R_{ref}, $V_{c,ref}$, etc. are known once the planet and the parking orbit have been selected, while V_∞ and/or ΔV_{imp_2} are known as a result of interplanetary calculations. The dimensionless variables v_∞^2, a_{po}, and v_j corresponding to the maneuver may then be found by means of equation (5) and used with figures 2 and 3 to determine values of f_v and θ_{ch}.

In some interplanetary studies (ref. 1), the results are presented in the form of values of v_∞ for each trip. Other studies, such as references 2 and 3, present the

TABLE I. - KEY TO POWERED ESCAPE AND CAPTURE TRAJECTORY DATA, CIRCULAR PARKING ORBITS, AND DIMENSIONLESS ARGUMENTS

Figure	Dependent variable	Maneuver	Jet velocity parameter, v_j	Dimensionless acceleration at parking orbit, a_{po}	Hyperbolic velocity parameter, v_∞^2
2(a)	f_v	Escape and capture	∞	0 - 5.0	-1 - 20
2(b)	θ_{ch}	Escape and capture	∞	0 - 5.0	-1 - 20
2(c)	f_v	Escape	5	0 - 5.0	-1 - 20
2(d)	f_v	Capture	5	0 - 5.0	-1 - 20
2(e)	f_v	Escape	2.5	0 - 5.0	-1 - 20
2(f)	f_v	Capture	2.5	0 - 5.0	-1 - 20
2(g)	f_v	Escape	1.0	0 - 1.0	-1 - 10
2(h)	f_v	Capture	1.0	0 - 5.0	-1 - 10
2(i)	θ_{ch}	Escape and capture	1.0	0.01 - 1.0	-1 - 10
2(j)	f_v	Escape	0.5	0 - 0.75	-1 - 10
2(k)	f_v	Capture	.5	0 - 5.0	-1 - 10
2(ℓ)	f_v	Escape	0.25	0 - 0.4	-1 - 10
2(m)	f_v	Capture	.25	0 - 10.0	-1 - 10

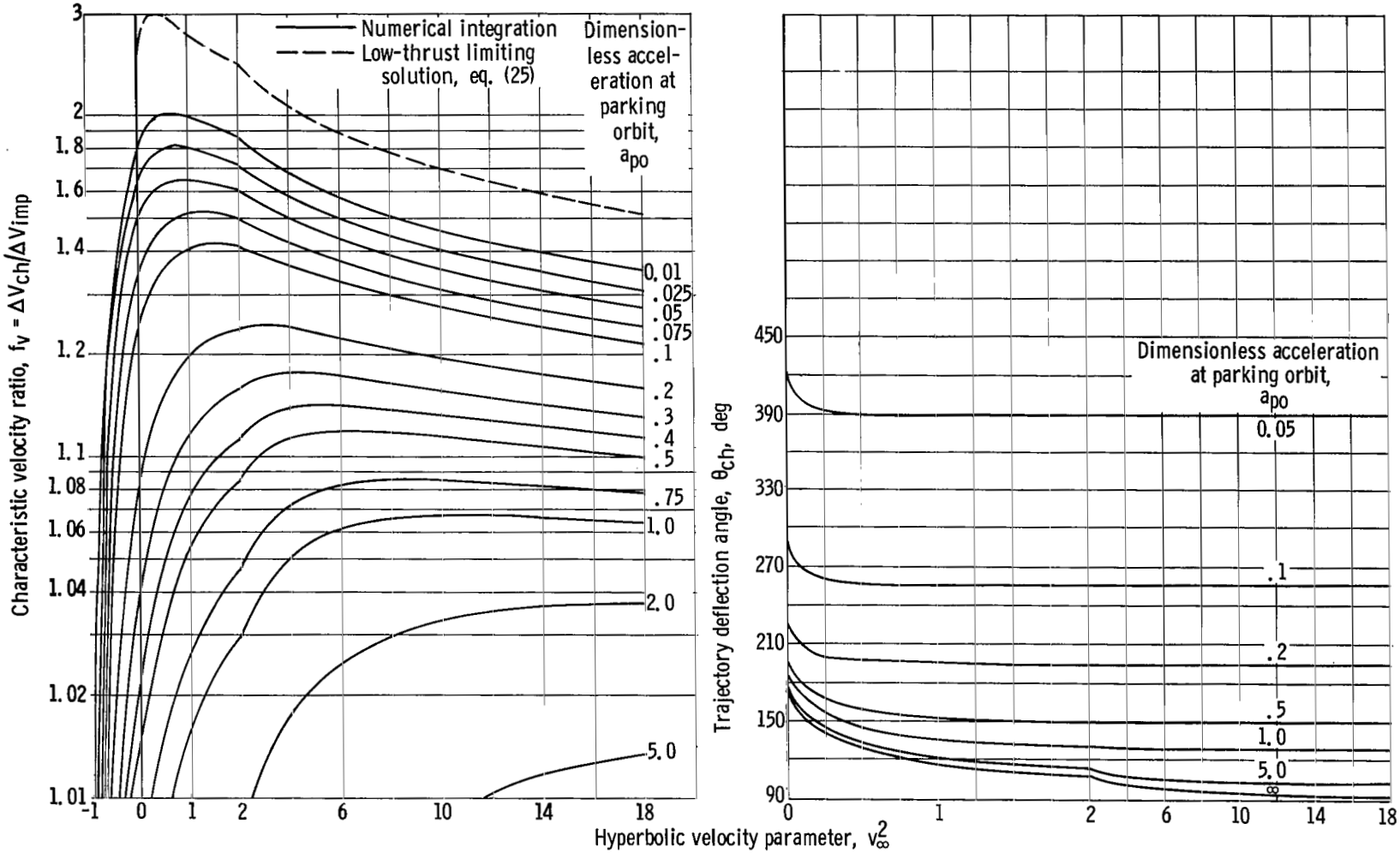

(a) Velocity correction factor; jet velocity parameter, ∞.

(b) Trajectory deflection angle; jet velocity parameter, ∞.

Figure 2. - Properties of escape and capture maneuvers. Circular parking orbit.

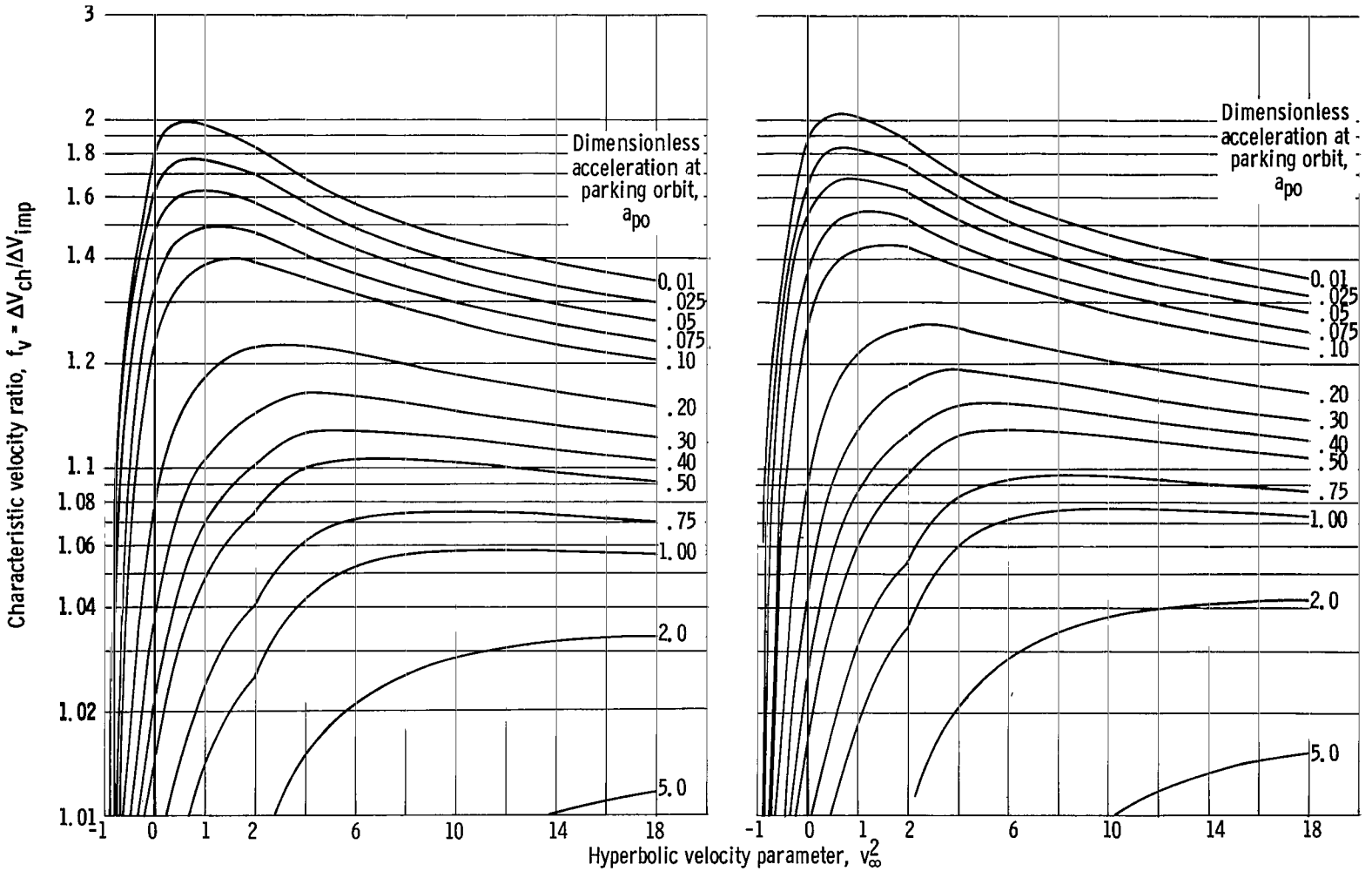

(c) Escape maneuver; jet velocity parameter, 5.0.

(d) Capture maneuver; jet velocity parameter, 5.0.

Figure 2. - Continued.

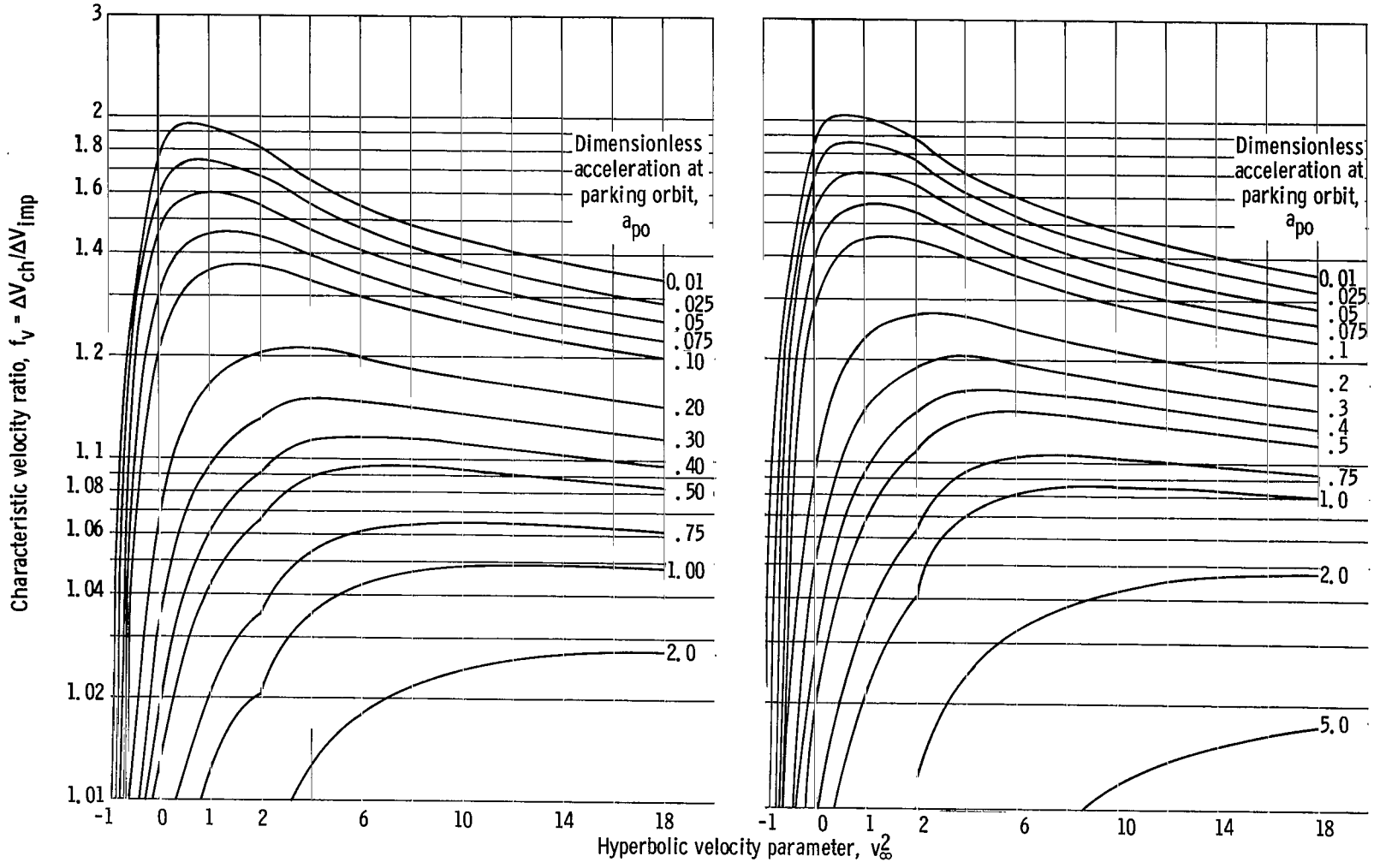

(e) Escape maneuver; jet velocity parameter, 2.5.

(f) Capture maneuver; jet velocity parameter, 2.5.

Figure 2. - Continued.

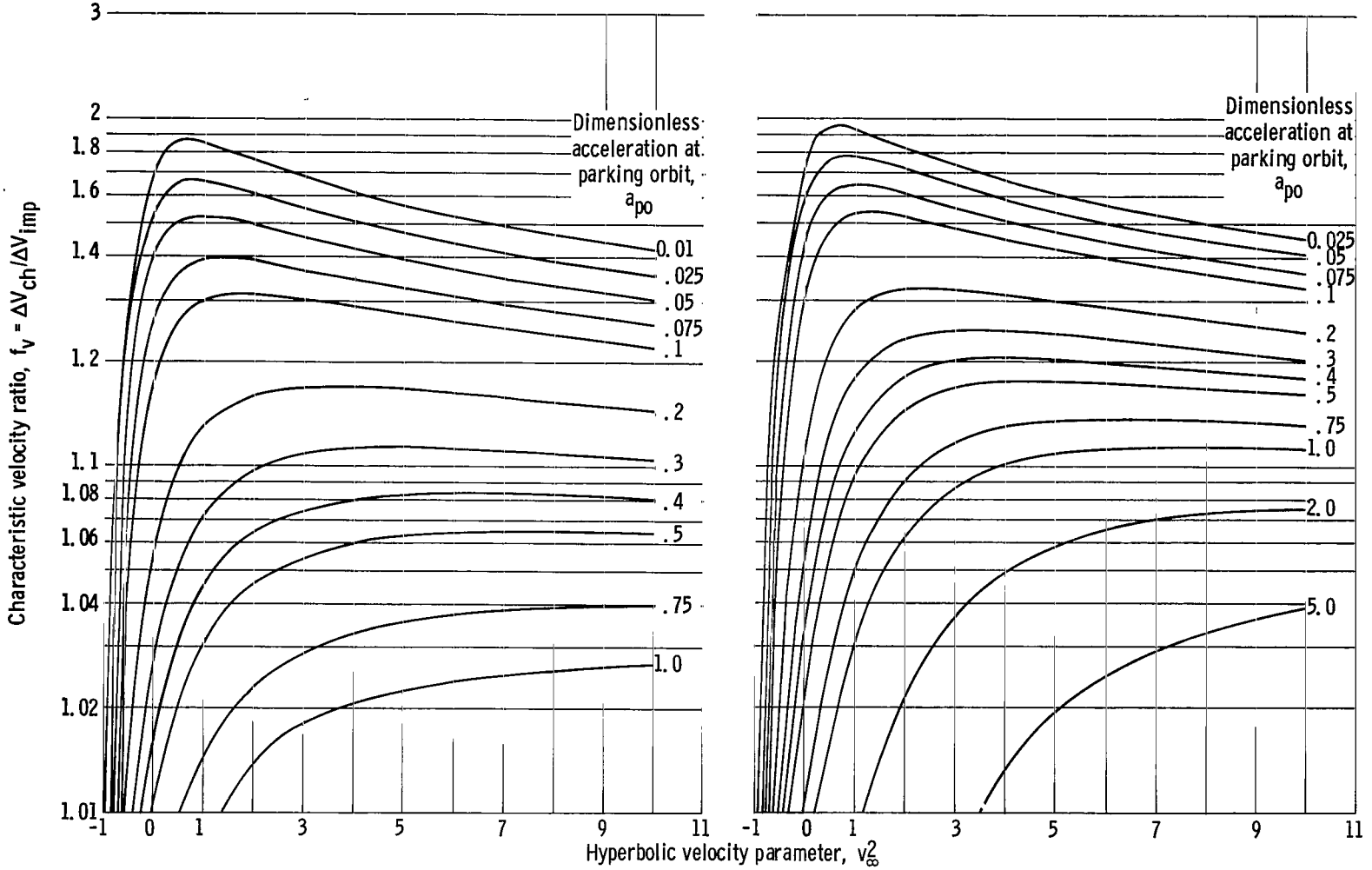

(g) Velocity correction factor; escape maneuver; jet velocity parameter, 1.0.

(h) Velocity correction factor, capture maneuver; jet velocity parameter, 1.0.

Figure 2. - Continued.

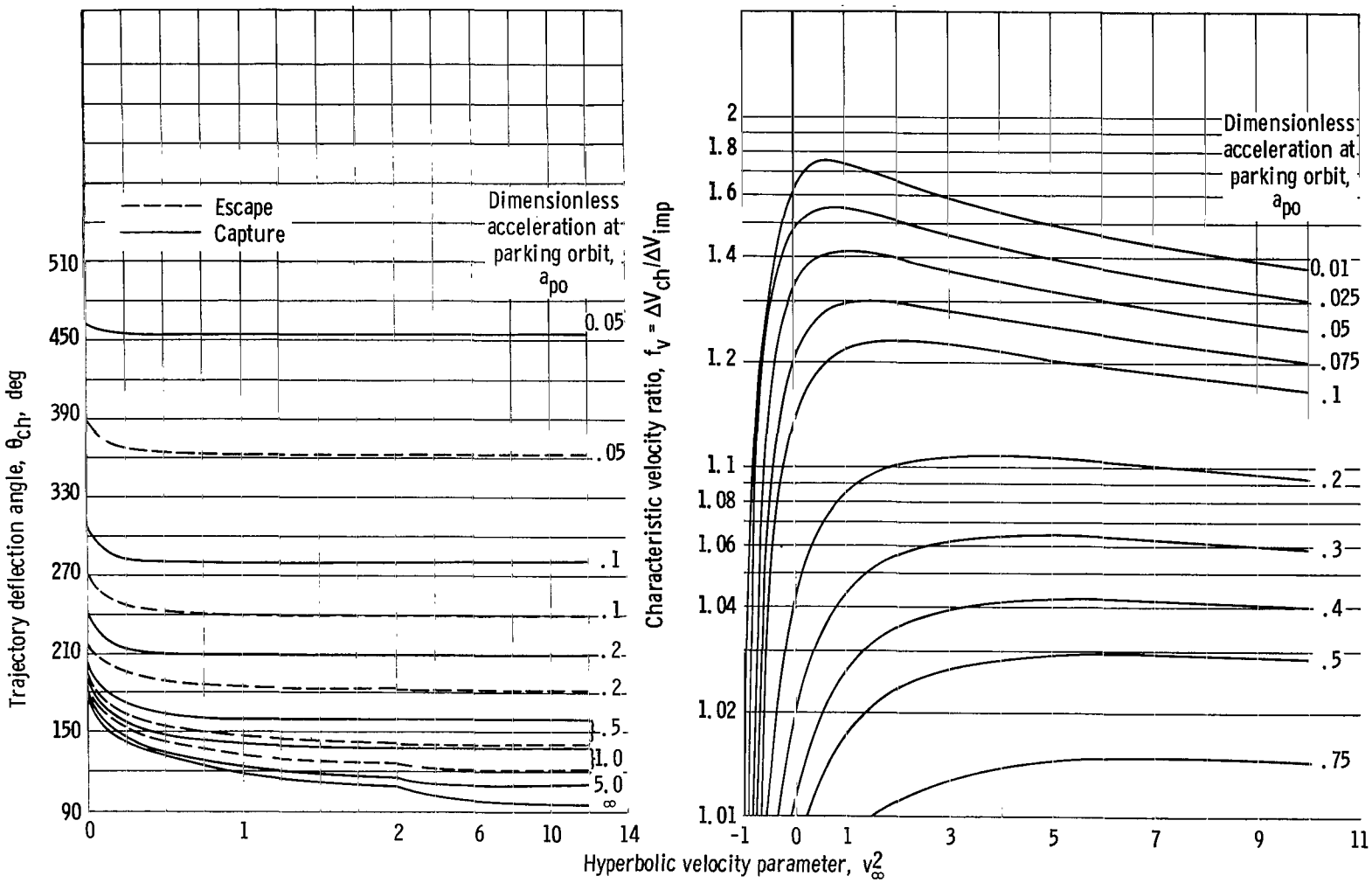

(i) Trajectory deflection angle; jet velocity parameter, 1.0.

(j) Escape maneuver; jet velocity parameter, 0.5.

Figure 2. - Continued.

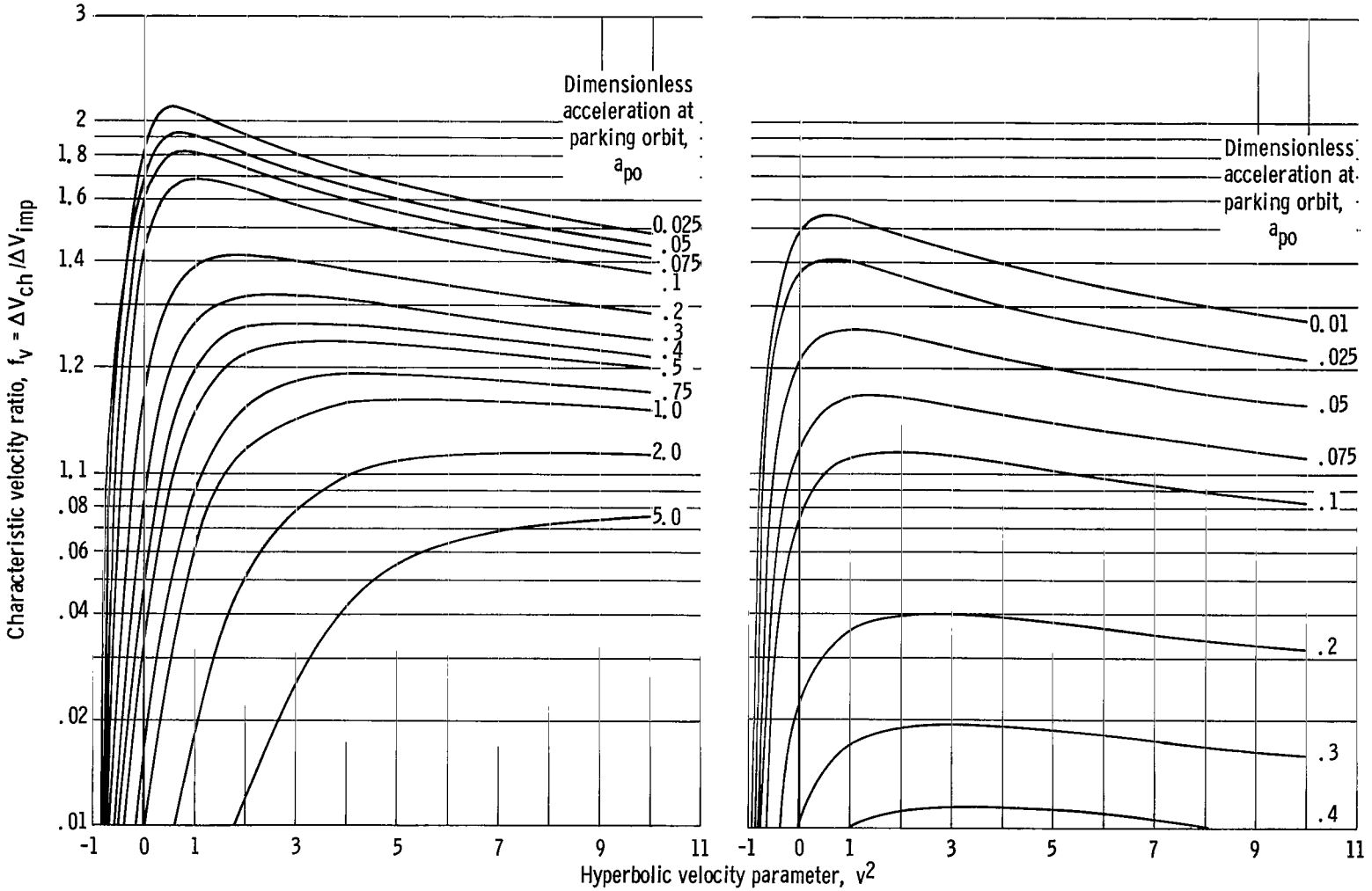

(k) Capture maneuver; jet velocity parameter, 0.5.

(l) Escape maneuver; jet velocity parameter, 0.25.

Figure 2. - Continued.

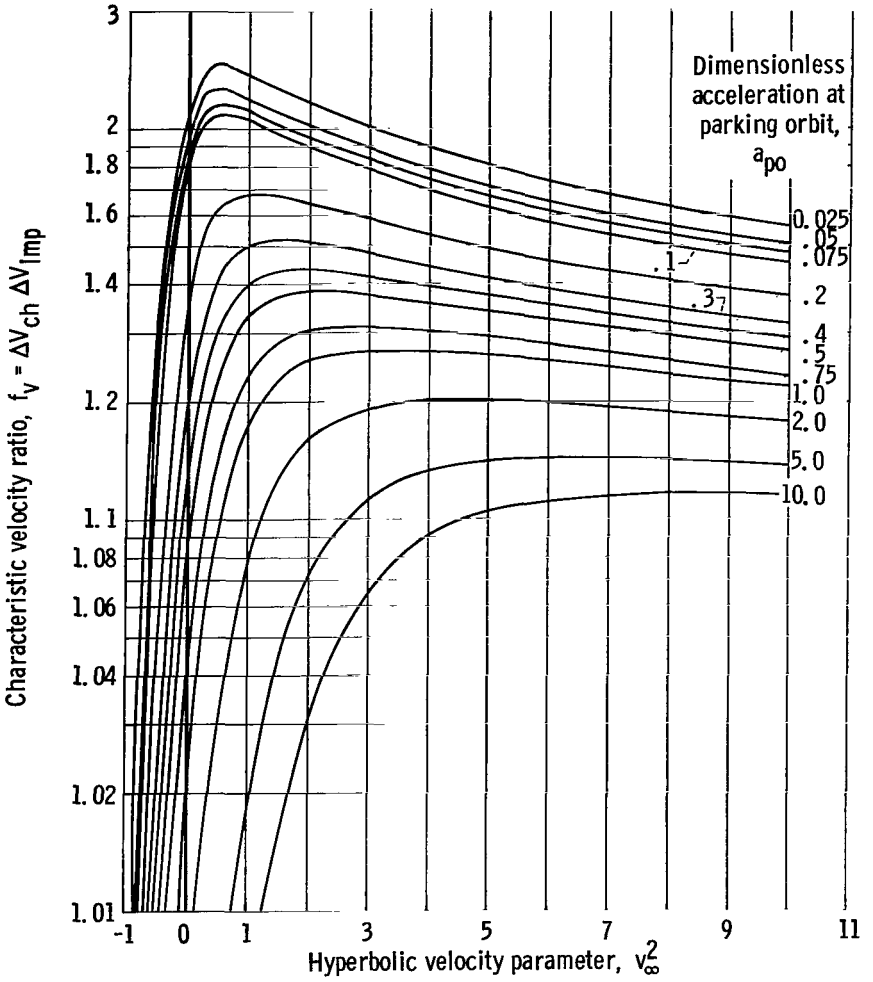

(m) Capture maneuver; jet velocity parameter, 0.25.

Figure 2. - Concluded.

TABLE II. - KEY TO POWERED ESCAPE AND CAPTURE TRAJECTORY DATA

[Elliptic parking orbits; parking orbit eccentricity, 0.9; optimum values of optimum orbital true anomaly, ν_{po}; optimum trajectory deflection angle, θ_{ch}.]

Figure	Dependent variable	Maneuver	Jet velocity parameter, v_j	Dimensionless acceleration at parking orbit, a_{po}	Hyperbolic velocity parameter, v_∞^2
3(a)	f_v	Escape and capture	∞	0 - 1.0	0 - 20
3(b)	θ_{ch}, ν_{po}	Escape and capture	∞	0 - 1.0	0 - 20
3(c)	f_v	Escape	5.0	0.01 - 1.0	0 - 20
3(d)	θ_{ch}, p_o	Escape	5.0	.01 - 1.0	0 - 20
3(e)	f_v	Capture	5.0	.01 - 1.0	0 - 20
3(f)	θ_{ch}, ν_{po}	Capture	5.0	.01 - 1.0	0 - 20
3(g)	f_v	Escape	2.5	0.01 - 1.0	0 - 20
3(h)	θ_{ch}, p_o	Escape	2.5	.01 - 1.0	0 - 20
3(i)	f_v	Capture	2.5	.01 - 1.0	0 - 20
3(j)	θ_{ch}, ν_{po}	Capture	2.5	.01 - 1.0	0 - 20
3(k)	f_v	Escape	1.0	0.01 - 1.0	0 - 12
3(l)	θ_{ch}, p_o	Escape	1.0	.01 - 1.0	0 - 12
3(m)	f_v	Capture	1.0	.01 - 1.0	0 - 12
3(n)	θ_{ch}, ν_{po}	Capture	1.0	.01 - 1.0	0 - 12
3(o)	f_v	Escape	0.5	0.01 - 1.0	0 - 12
3(p)	θ_{ch}, ν_{po}	Escape	.5	.01 - 1.0	0 - 12
3(q)	f_v	Capture	.5	.01 - 1.0	0 - 12
3(r)	θ_{ch}, ν_{po}	Capture	.5	.01 - 1.0	0 - 12
3(s)	f_v	Escape	0.25	0.01 - 0.2	0 - 8
3(t)	θ_{ch}, ν_{po}	Escape	.25	.01 - .2	0 - 8
3(u)	f_v	Capture	.25	.01 - 10.0	0 - 8
3(v)	θ_{ch}, ν_{po}	Capture	.25	.01 - 10.0	0 - 8

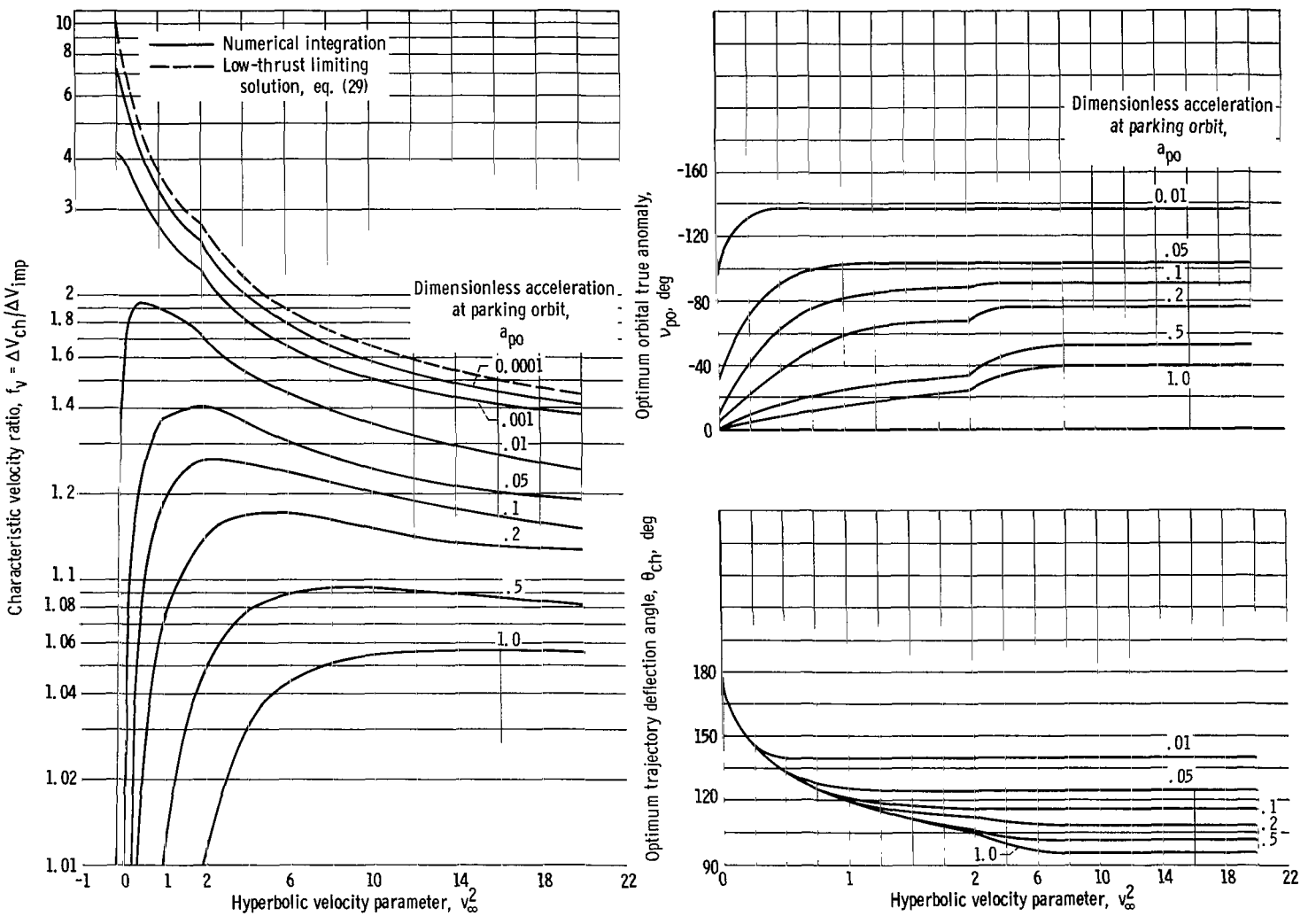

(a) Velocity correction factor; jet velocity parameter, ∞.

(b) Optimum deflection angle and true anomaly; jet velocity parameter, ∞.

Figure 3. - Properties of escape and capture maneuvers. Elliptic parking orbit; parking orbit eccentricity, 0.9.

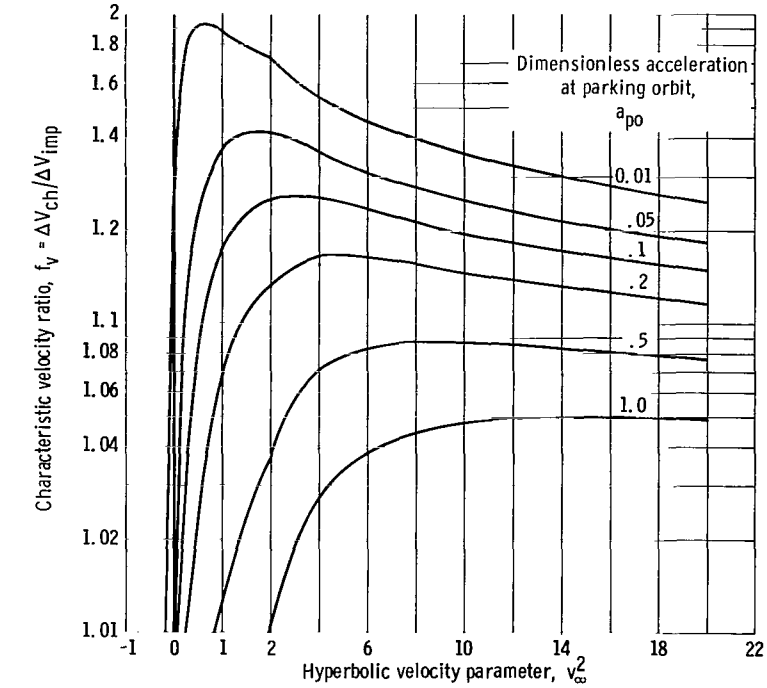

(c) Escape maneuvers; jet velocity parameter, 5.0.

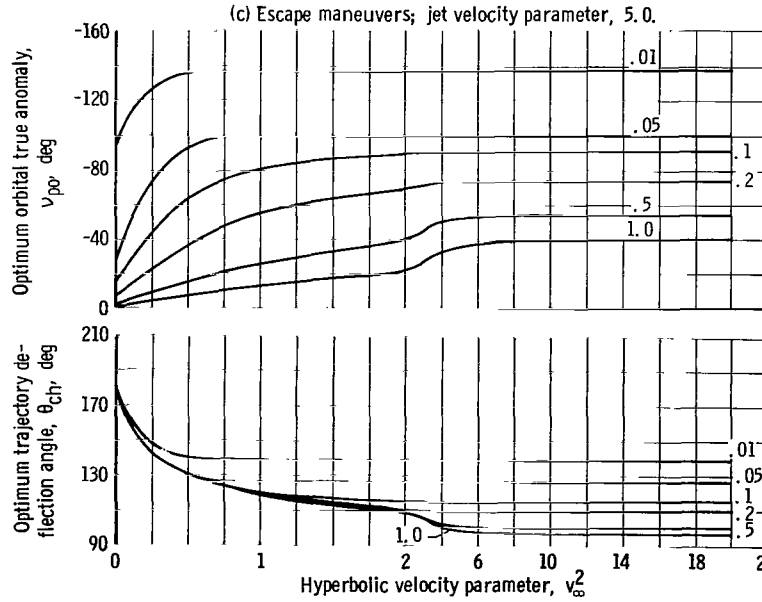

(d) Optimum deflection angle and true anomaly, escape; jet velocity parameter, 5.0.

Figure 3. - Continued.

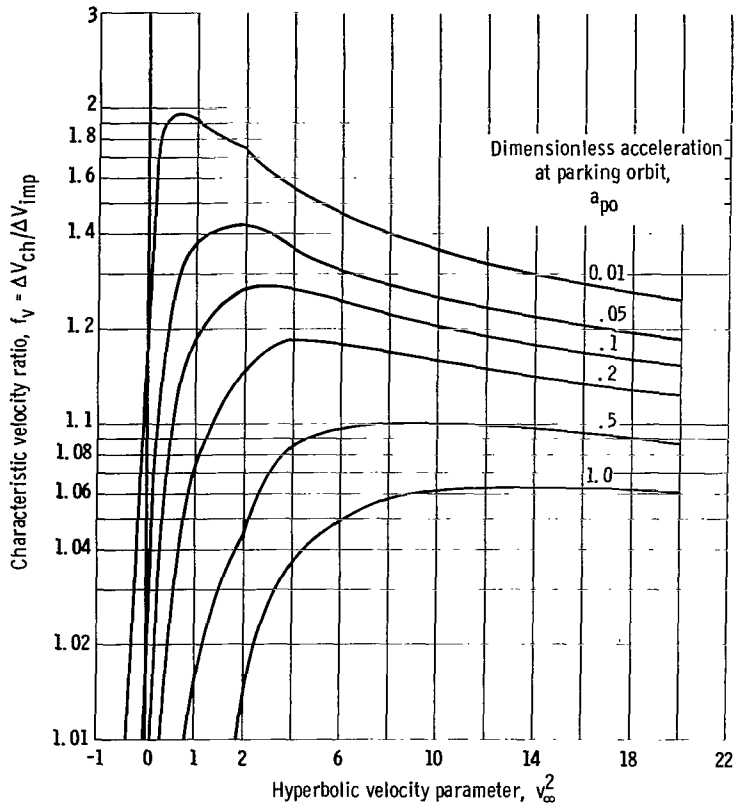

(e) Capture maneuvers; jet velocity parameter, 5.0.

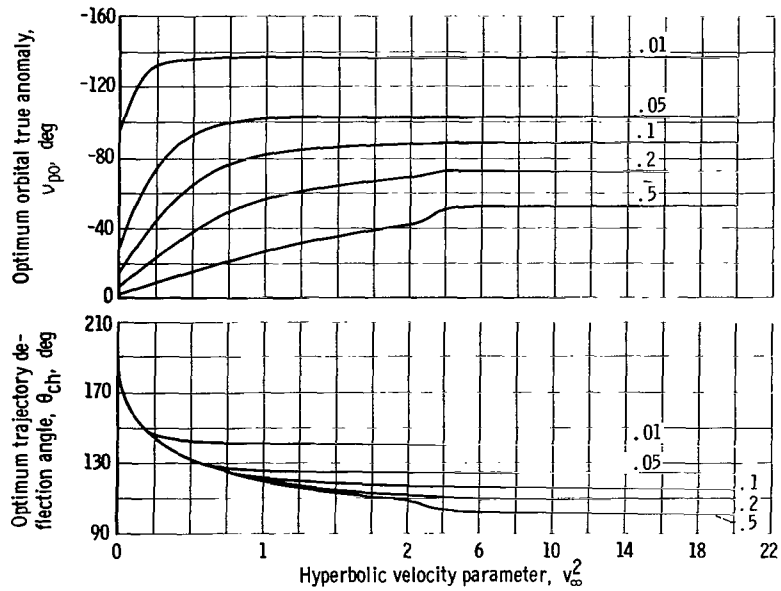

(f) Optimum deflection angle and true anomaly, capture; jet velocity parameter, 5.0.

Figure 3. - Continued.

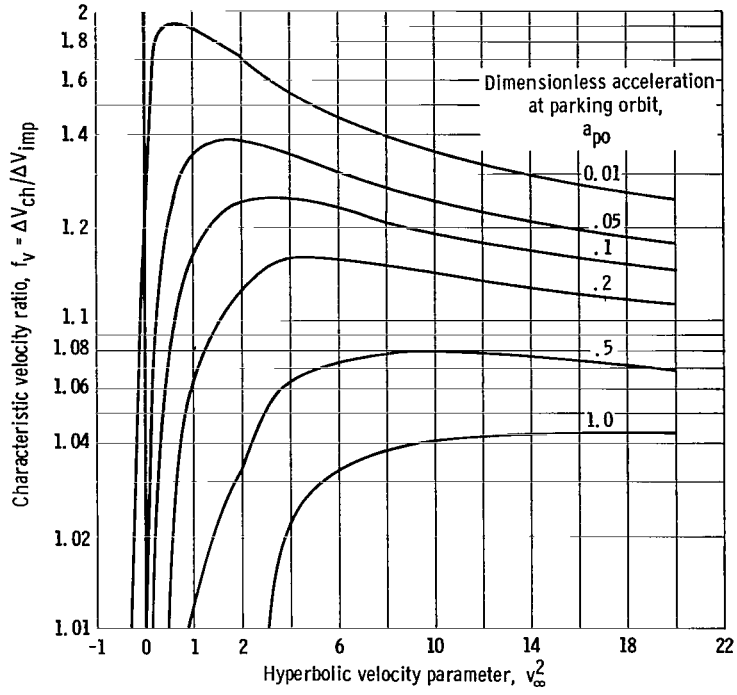

(g) Escape maneuvers; jet velocity parameter, 2.5.

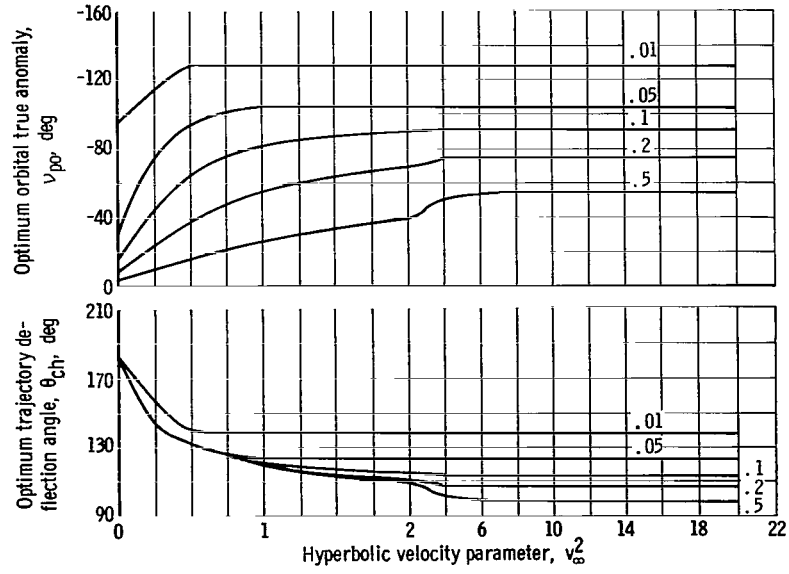

(h) Optimum deflection angle and true anomaly, escape; jet velocity parameter, 2.5.

Figure 3. - Continued.

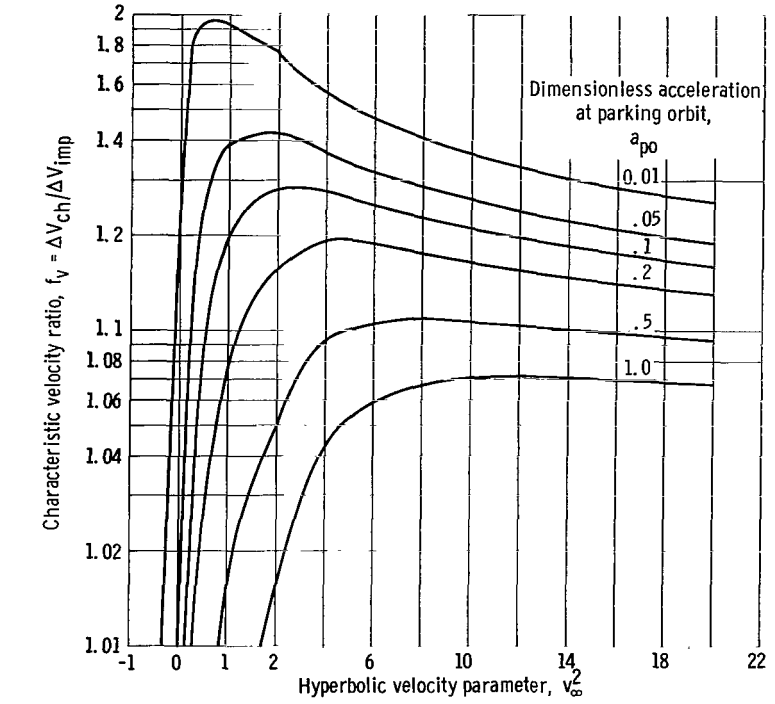

(i) Capture maneuvers; jet velocity parameter, 2.5.

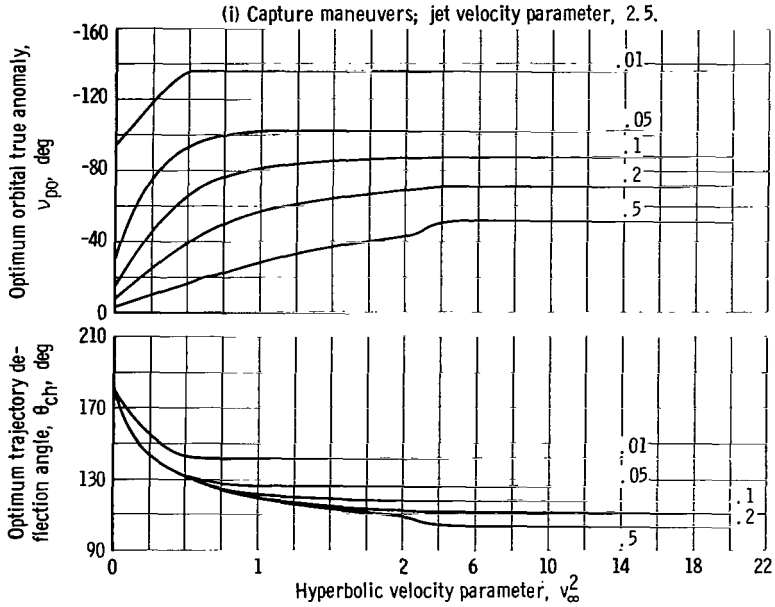

(j) Optimum deflection angle and true anomaly, capture; jet velocity parameter, 2.5.

Figure 3. - Continued.

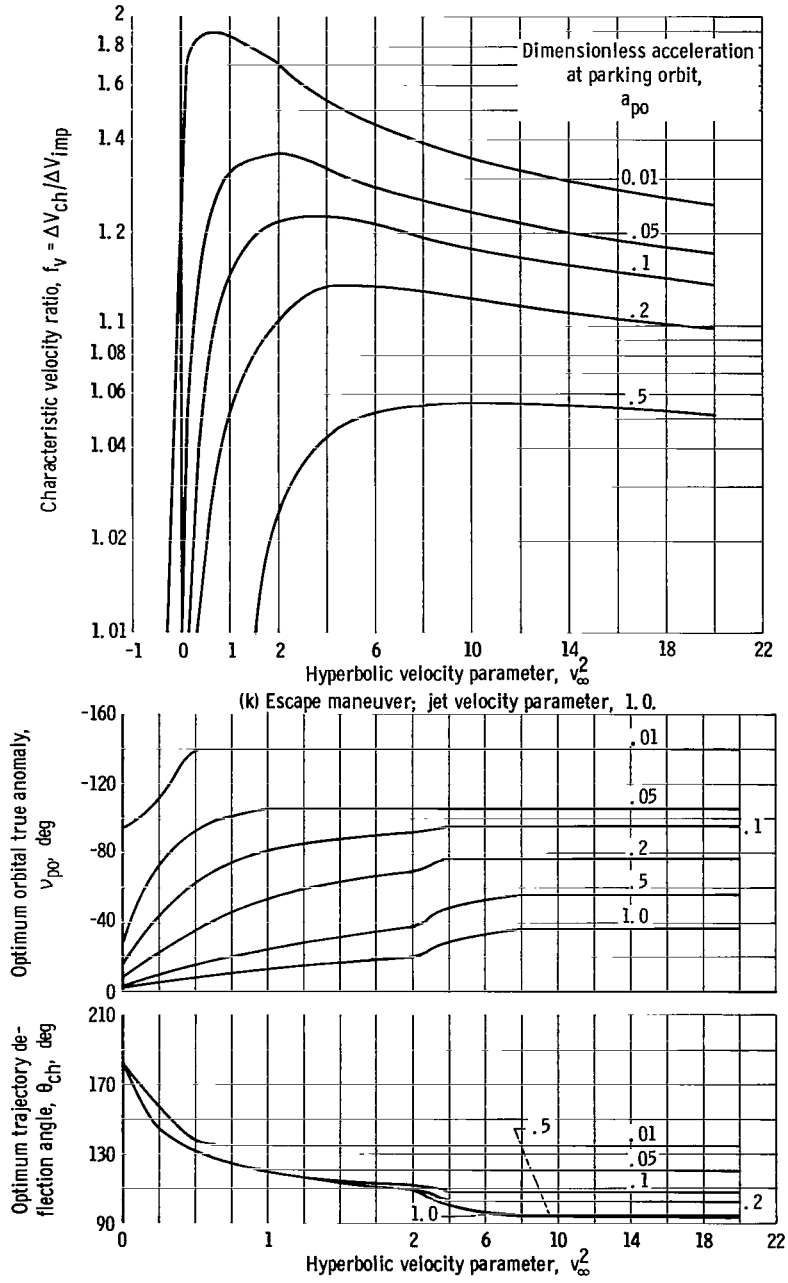

(k) Escape maneuver; jet velocity parameter, 1.0.

(l) Optimum deflection angle and true anomaly, escape; jet velocity parameter, 1.0.

Figure 3. - Continued.

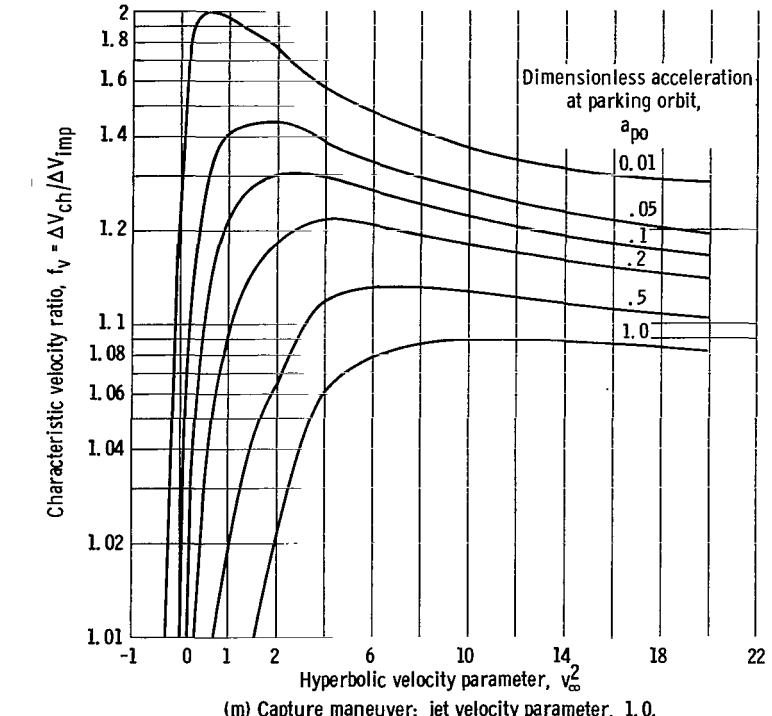

(m) Capture maneuver; jet velocity parameter, 1.0.

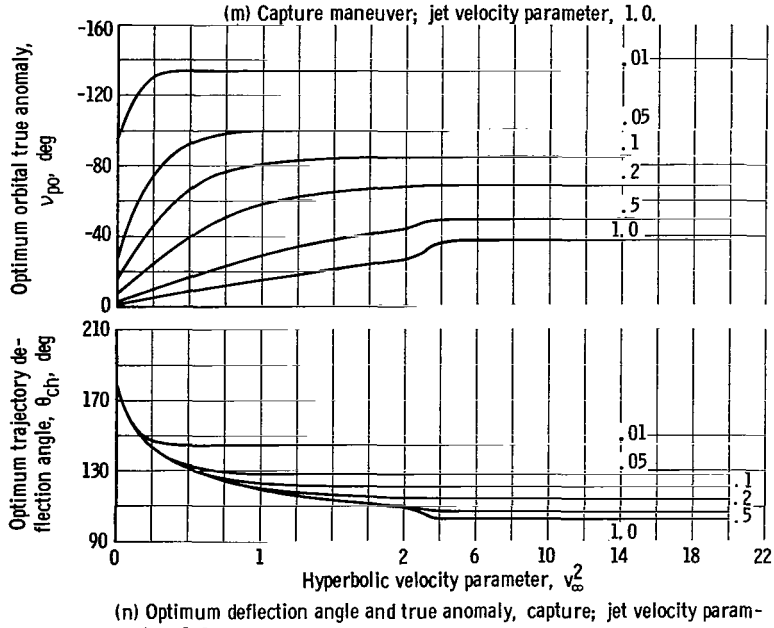

(n) Optimum deflection angle and true anomaly, capture; jet velocity parameter, 1.0.

Figure 3. - Continued.

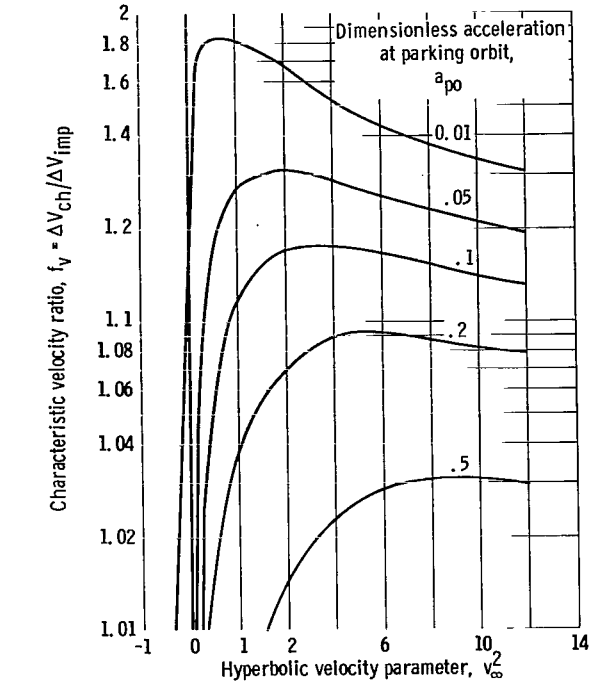

(o) Escape maneuver; jet velocity parameter, 0.5.

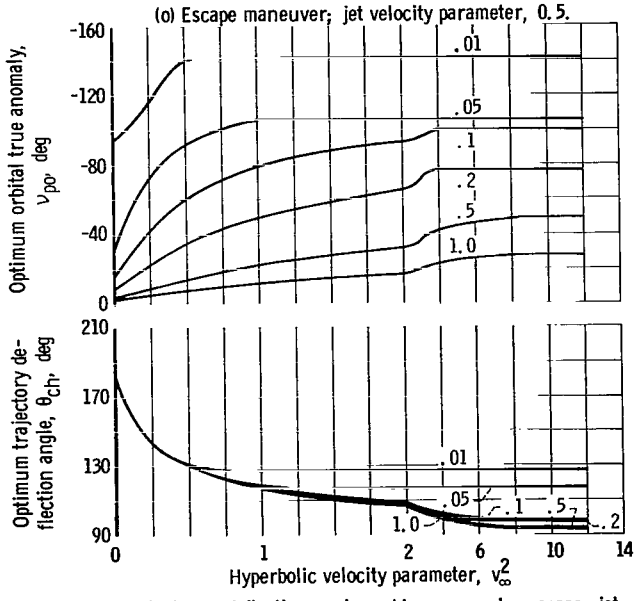

(p) Optimum deflection angle and true anomaly, escape; jet velocity parameter, 0.5.

Figure 3. - Continued.

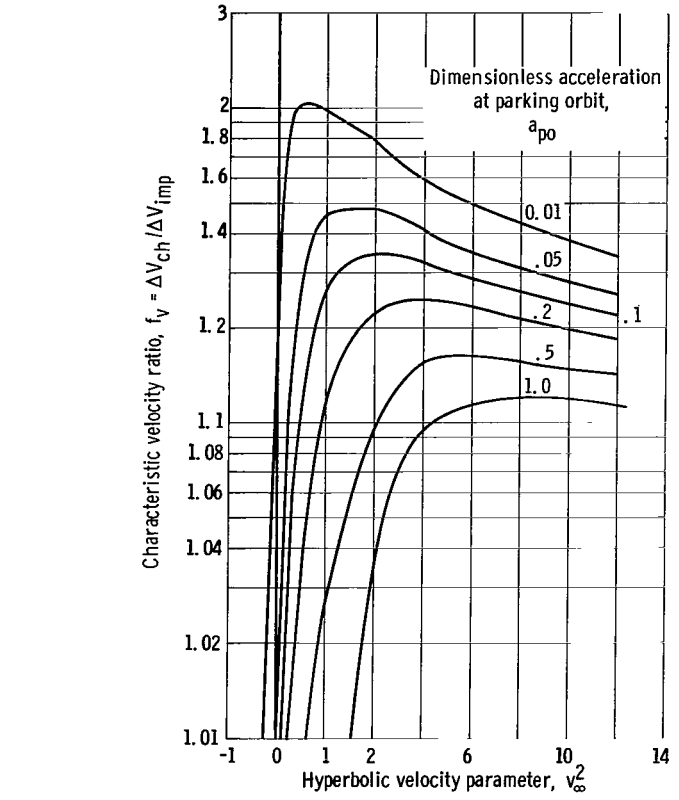

(q) Capture maneuver; jet velocity parameter, 0.5.

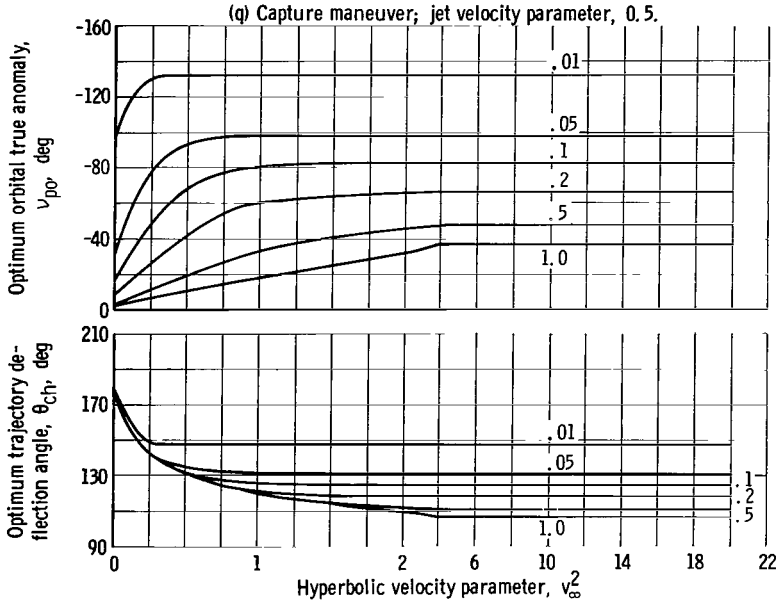

(r) Optimum deflection angle and true anomaly, capture; jet velocity parameter, 0.5.

Figure 3. - Continued.

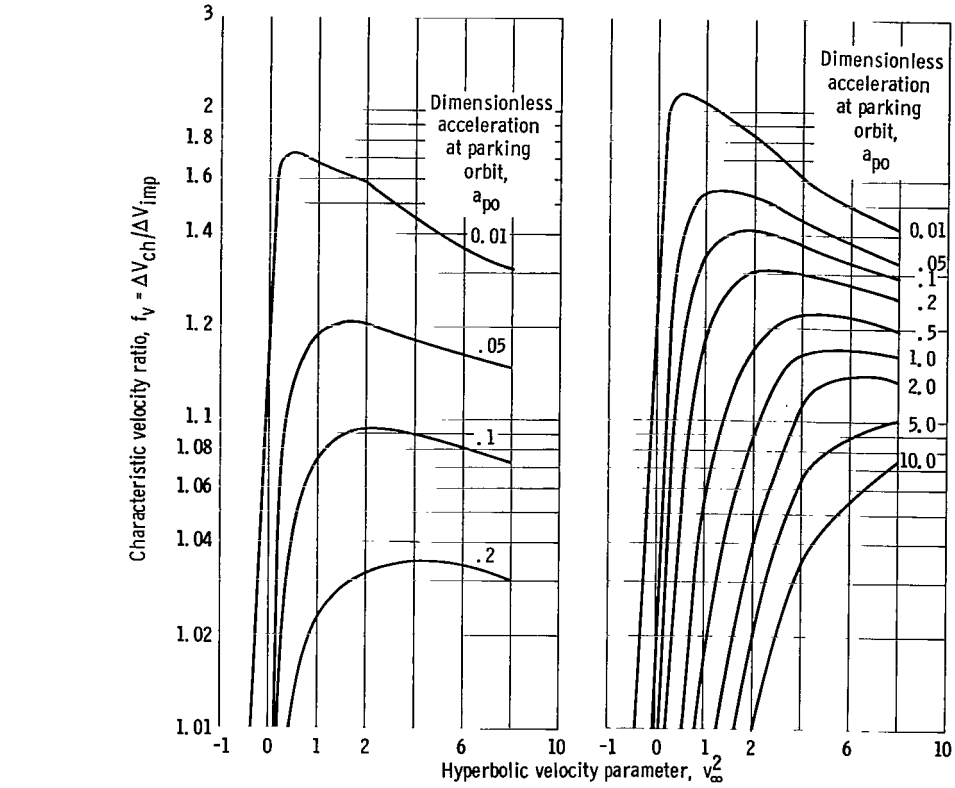

(s) Escape maneuver; jet velocity parameter, 0.25.

(u) Capture maneuver; jet velocity parameter, 0.25.

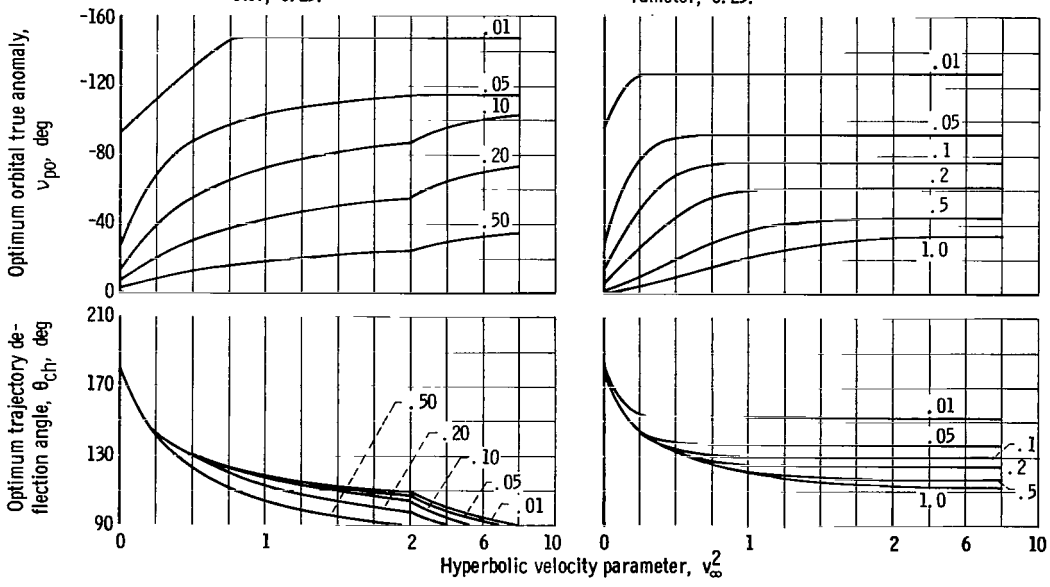

(t) Optimum deflection angle and true anomaly, escape, jet velocity parameter, 0.25.

(v) Optimum deflection angle and true anomaly, capture; jet velocity parameter, 0.25.

Figure 3. - Concluded.

equivalent impulsive velocity increment ΔV_{imp} necessary to leave or enter an assumed circular parking orbit at 1.1 planet radii. In figure 4(a), v_∞^2 is plotted as a function of ΔV_{imp} (in miles/sec) for each planet of the solar system, with $R_{po} = 1.1\ R_{pl}$. Figure 4(b) gives the conversion between ΔV_{imp} and v_∞ in EMOS (i.e., in units of the Earth's mean orbital speed, 18.5058 miles/sec). In figure 4(c), a_{po} is shown in terms of A_{po} (in units of Earth surface gravity, 32.17 ft/sec^2), again assuming $R_{po} = 1.1\ R_{pl}$. The dimensionless jet velocity parameter v_j is shown in figure 4(d) as a function of specific impulse I (in sec).

As an example, suppose that it is desired to attain a value of $V_\infty = 0.2$ EMOS from a circular Earth-centered parking orbit ($R_{po} = 1.1\ R_\oplus$) using a chemical rocket with I = 385 seconds and A_i (= A_{po}) = 9 feet per second^2 or 0.27 $G_{\oplus, s}$. From figures 4(a) and (b) it may be seen that the corresponding value of ΔV_{imp} is about 3 miles per second and v_∞^2 is approximately 0.7. Also, $a_{po} \approx 0.3$ and $v_j \approx 0.5$, as noted in figures 4(c) and (d). If these values ($v_\infty^2 = 0.7$, $a_{po} = 0.3$, $v_j = 0.5$) of the dimensionless arguments are used, the corresponding value of f_v may be found in figure 2(j) (p. 25) - that is, $f_v = 1.037$. Thus, the actual characteristic velocity increment is $\Delta V_{ch} \approx 1.037 \times 3$ or 3.11 miles per second, and the propellant fraction is

$$m_p = 1 - \exp \frac{-3.11 \times 5280}{385 \times 32.17}$$

or 0.735. Exactly the same procedure would be used for a capture maneuver with a specified value of A_{bo} (rather than A_i); when figure 2(k) is used, the value of f_v for the arguments enumerated above is seen to be $f_v = 1.230$.

On the other hand, if it is desirable to study capture maneuvers on the basis of given values of A_i, or to

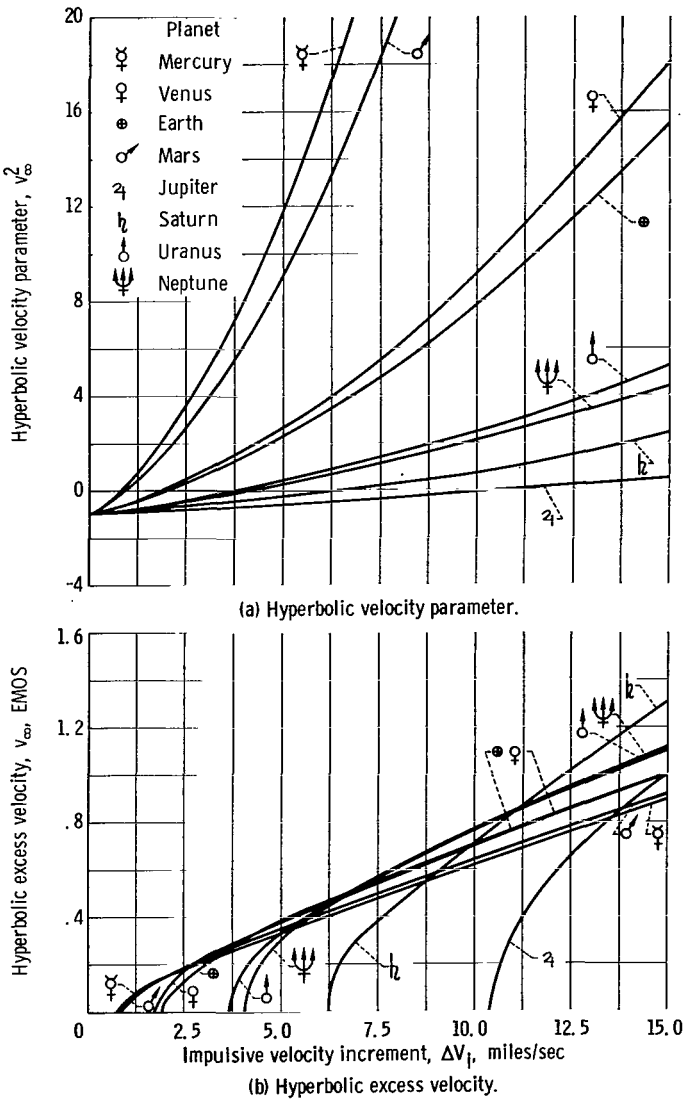

Figure 4. - Scaling of dimensionless parameters for planets of the solar system.

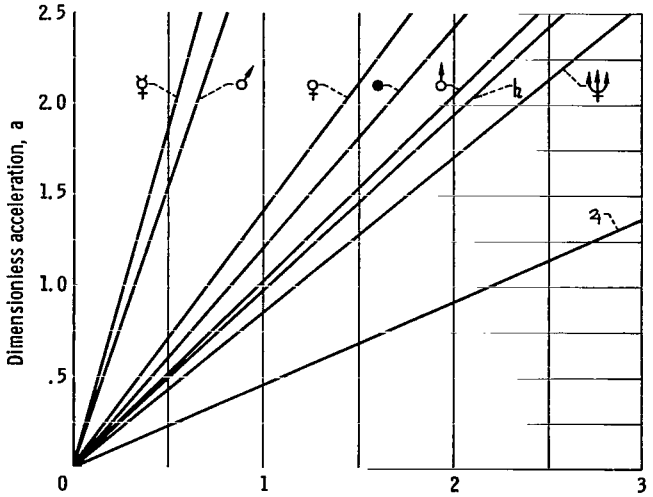

(c) Acceleration parameter.

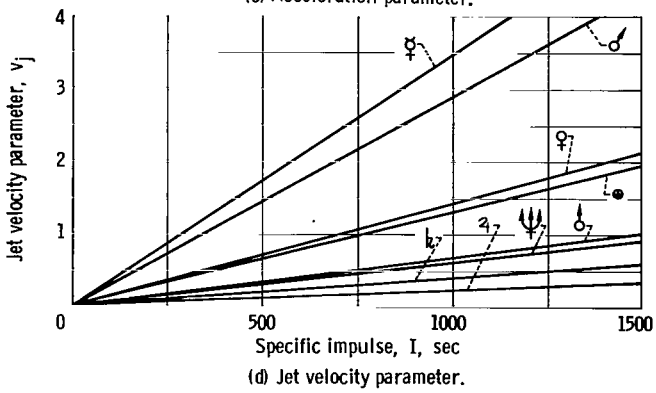

(d) Jet velocity parameter.

Figure 4. - Concluded.

study escape maneuvers with given values of A_{bo}, it is necessary to solve equation (10) by iteration. For instance, to find f_v for the previous capture maneuver with A_i = 9 feet per second^2 requires the following steps:

(1) The v_∞^2 and v_j are as given previously.

(2) A trial value of a_{po}(= a_{bo}) is assumed.

(3) The f_v is found in the data and a trial value of m_p is computed by using equations (3) and (15).

(4) A new value of a_{po} (= a_{bo}) is computed from equation (10a) - compare with step (2).

(5) Steps (2) to (4) are repeated using the new value of a_{bo} from (4) until convergence is obtained.

A similar procedure is used to find the characteristics of escape maneuvers with given values of A_{bo}.

Dimensional Data

For studies which involve repetitive but similar calculations, it is convenient to perform the previous conversion, interpolation, and iteration in advance. This yields working charts that apply to a specific planet and parking orbit, and to ranges of A_i (or A_{bo}) and I which are of particular interest. As an example, the preceding dimensionless circular orbit data have been used to generate a series of working charts that describe nuclear rocket maneuvers near Earth, Venus, and Mars (figs. 5, 6, and 7, respectively). Values of f_v are plotted against ΔV_{imp}, assuming a circular orbit radius of 1.1 planet radii for values of A_i ranging from 0.1 to 1.0 $G_\oplus$ and specific impulses of 900 seconds (solid curves) and 700 seconds (dashed curves). Part (a) of each of these figures represents escape maneuvers while captures are shown in part (b). It is noted that the captures are correlated on the basis of the initial acceleration A_i.

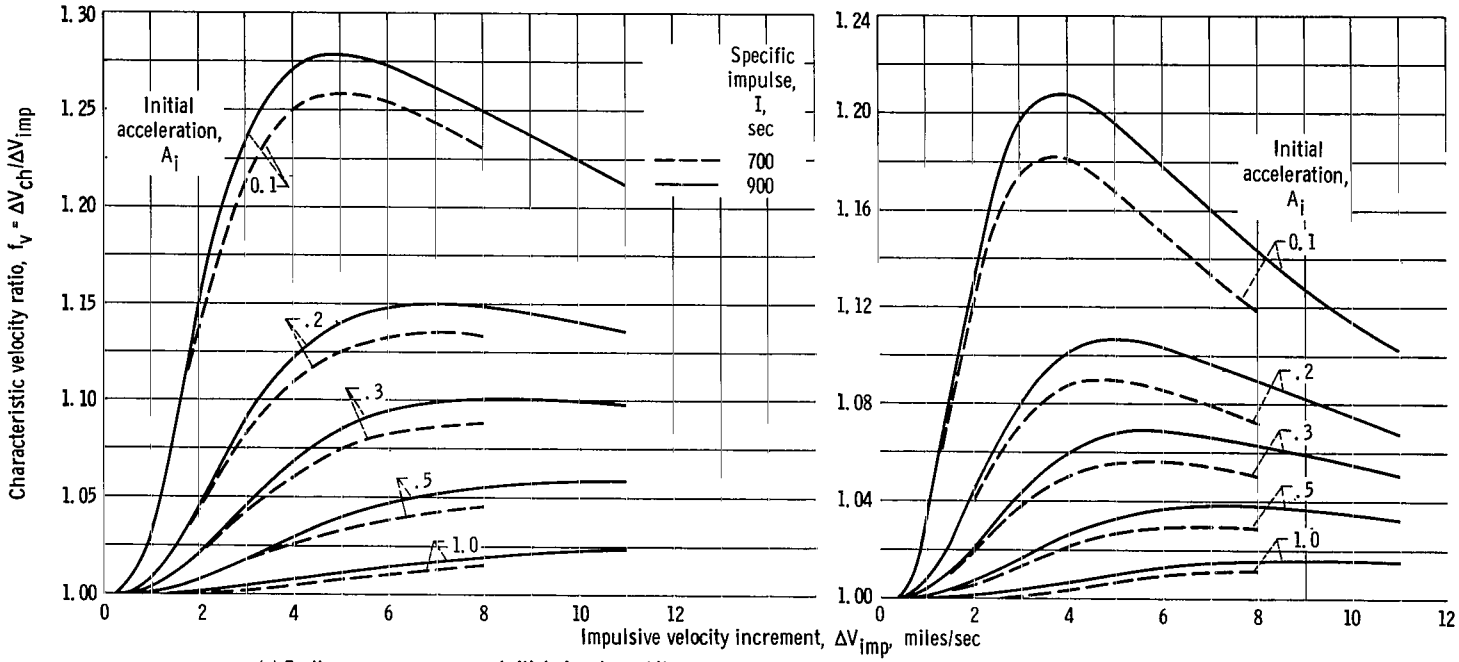

(a) Earth escape maneuver. Initial circular orbit.

(b) Earth capture maneuver. Final circular orbit.

Figure 5. - Characteristic velocity ratio at Earth. Constant tangential thrust; altitude, 1.1 planet radii.

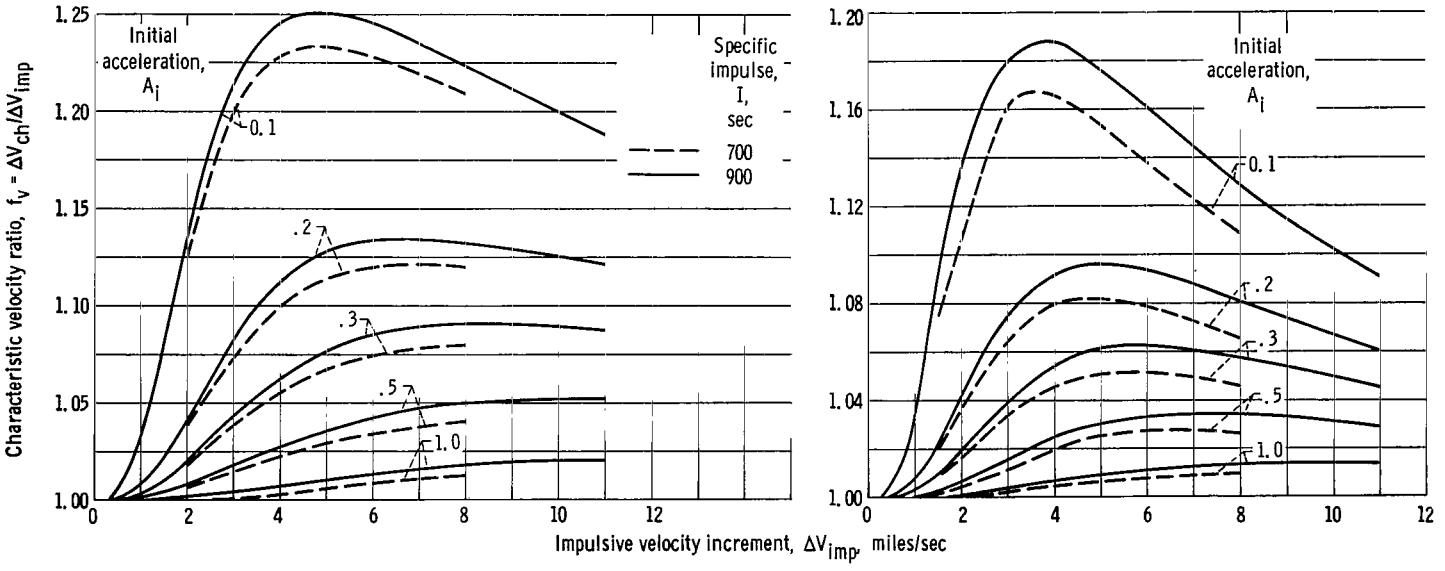

(a) Venus escape maneuver. Initial circular orbit.

(b) Venus capture maneuver. Final circular orbit.

Figure 6. - Characteristic velocity ratio at Venus. Constant tangential thrust; altitude, 1.1 planet radii.

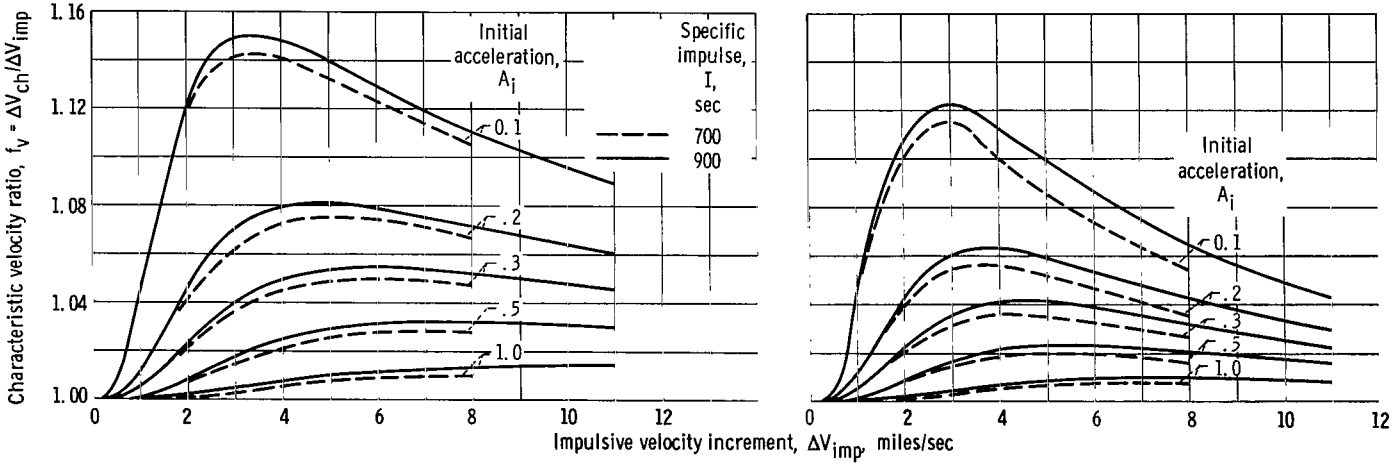

(a) Mars escape maneuver. Initial circular orbit.

(b) Mars capture maneuver. Final circular orbit.

Figure 7. - Characteristic velocity ratio at Mars. Constant tangential thrust; altitude, 1.1 planet radii.

DISCUSSION

The preceding results define the essential dynamic and geometric properties of a very wide range of optimum-angle finite-thrust trajectories. This section is intended to interpret the behavior of these results by examining the role of each of the independent variables. The effects of v_∞^2, a_{po}, and v_j are first considered in terms of circular orbits. The additional variables (v_∞ and e_{po}) associated with elliptic orbits are then discussed, and finally the circular and elliptic orbit results are compared.

Circular Orbits

Effects of hyperbolic velocity parameter v_∞^2. - The characteristic velocity ratio f_v is shown as a function of v_∞ (and a_{po}) in figure 2(a) (p. 21) for escape or capture maneuvers with $v_j = \infty$ (for instance). The uppermost curve on this graph is the low-thrust limiting solution expressed in equation (25). This curve gives the upper bound for f_v as a function of v_∞; the peak value of $f_v = 3$ occurs at $v_\infty = 0.25$, and thereafter f_v declines as v_∞ increases. For trajectories with intermediate thrust, the f_v function behaves in qualitatively the same way. The peak value of f_v, however, decreases and occurs at higher values of v_∞^2 as a_{po} is increased. For instance, with $a_{po} = 0.01$, $f_{v,\,max} = 2$ at $v_\infty^2 = 0.65$. As a_{po} approaches the high-thrust regime, the peak becomes low, very broad, and occurs at high values of v_∞^2. Although not shown on the figure, $f_v \to 1.0$ for all values of a_{po} when $v_\infty^2 \to -1$ (i.e., when $\Delta v_{imp} \to 0$).

The characteristic central angle θ_{ch} is also influenced by v_∞^2 as illustrated in figure 2(b) (p. 21). For impulsive thrust ($a_{po} = \infty$), θ_{ch} is given by equation (16); it varies downward from a maximum of 180° at $v_\infty^2 = 0$, asymtotically approaching a lower bound of 90° for large v_∞^2. For finite values of a_{po}, the behavior is similar; the greatest value of θ_{ch} corresponds to $v_\infty^2 = 0$, with a rapid approach to a lower bound as v_∞^2 increases. The larger values of θ_{ch} at low v_∞^2 are due to the fact that low energy trajectories remain within the sphere of influence a longer time and thus are more strongly influenced by gravity.

Effects of orbit acceleration parameter a_{po}. - Although θ_{ch} is a bounded function of v_∞ for given a_{po}, it is not a bounded function of a_{po} for given v_∞. This may be inferred from figure 2(b) and is further illustrated in figure 8, in which θ_{ch} is plotted directly against a_{po} for several typical maneuvers. The large values of θ_{ch} at low a_{po} are due to the large value of θ_{bo} associated with low-thrust spiraling.

The behavior of f_v as a function of a_{po} is illustrated in figure 9 for several typical maneuvers. It is clear that f_v is bounded between the impulsive ($f_v = 1$) and ultra low-thrust limits. The asymptotic value in the latter case is given in terms of v_∞^2 by equa-

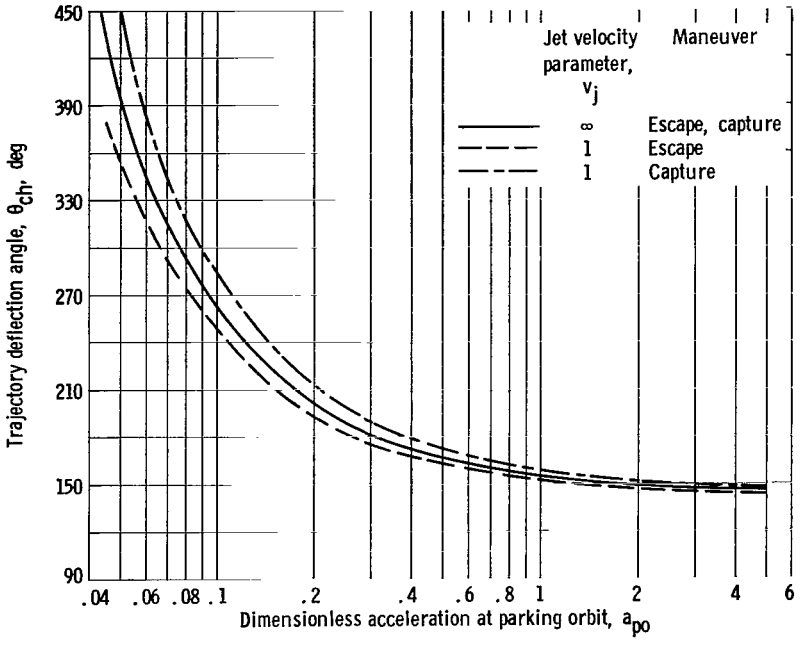

Figure 8. - Effect of orbit acceleration parameter on trajectory deflection. Circular parking orbit; hyperbolic velocity parameter, 0.25.

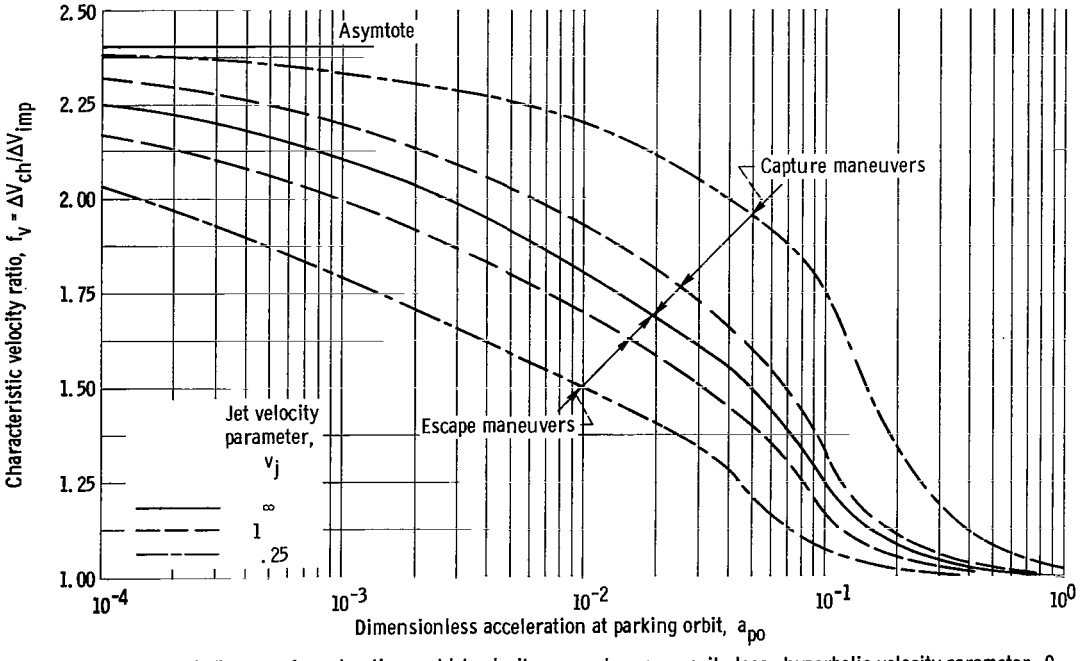

Figure 9. - Influence of acceleration and jet velocity parameters on gravity loss; hyperbolic velocity parameter, 0.

tion (25). It may be observed that f_v varies most rapidly with a_{po} in the range $0.03 \leq a_{po} \leq 0.3$. This range includes the thrust to weight ratios that are normally of interest for vehicles using nuclear rocket propulsion and low parking orbits.

The characteristic behavior of f_v may be understood by considering how the mean tangential velocity component $\langle v \cos u \rangle$ varies with a_{po} and v_∞^2. (For tangential thrust, only $\langle v \rangle$ need be considered.) When equation (32) is used, the maximum value of f_v, with given v_∞^2, occurs for minimum $\langle v \rangle$. Figure 10 depicts the velocity history of a typical set of tangential-thrust maneuvers (escapes from a circular orbit with $v_j = 1$). The path velocity v during the thrusting phase is plotted against the cumulative mass ratio M_i/M_{bo} on the logarithmic scale, and against Δv_{ch} on the linear scale. Each solid curve represents maneuvers with a given value of a_{po}. The upper straight line represents impulsive maneuvers, while the lower curve denotes the zero-thrust limit. Loci of constant v_∞ are shown in dashed lines. For high but finite acceleration, v increases monotonically with Δv_{ch}, although not as rapidly as in the impulsive case. At low acceleration, however, v actually decreases initially, and only begins to increase again after a fairly high value of v_∞^2 has been attained. It is clear that for any final

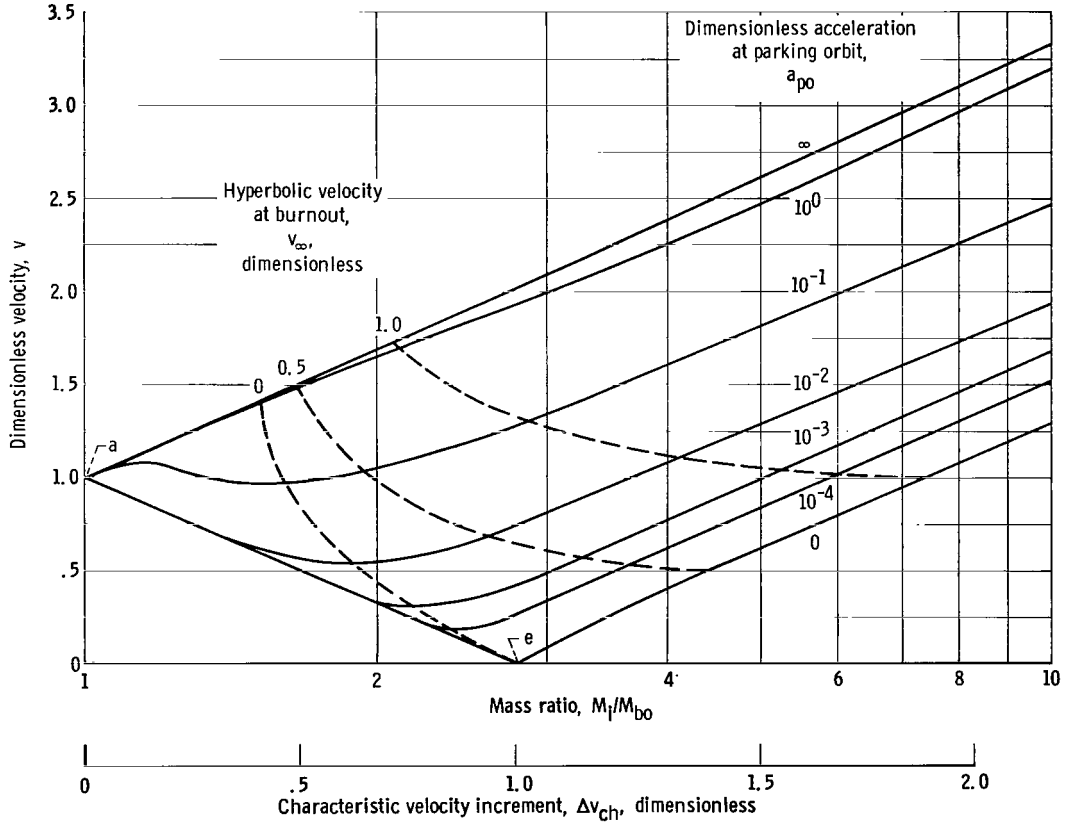

Figure 10. - Velocity to mass ratio history for dimensionless escape. Jet velocity parameter, 1.0.

value of v_∞, $\langle v \rangle$ decreases as a_{po} decreases and this accounts for the fact that f_v increases as a_{po} decreases.

The location and magnitude of the peak value of f_v as a function of v_∞^2 may be predicted by determining $\langle v \rangle$ (for example, by graphical means) from figure 10. For instance, in the low-thrust limit (lowest curve in fig. 10), it is readily verified that the minimum value of $\langle v \rangle$ (≈ 0.417)[1] occurs when $\Delta v_{ch} \approx 1.5$ and $v_\infty \approx 0.5$. These values in equation (4) yield $f_v = 3$ in agreement with both equations (25) and (32).

Effects of jet velocity parameter v_j. - Variations in v_∞^2 and a_{po} have similar effects on escape and capture maneuvers. The effect of v_j, however, is qualitatively different for the two types of maneuvers when they are compared on the basis of equal values of a_{po}, as shown in figure 11. The reason for this behavior can be found by inspection of equations (9a) and (9b). That is, for finite v_j, $a(\tau)$ increases continuously during an escape maneuver; the lower the values of v_j the greater the increase of $a(\tau)$. As $v_j \to 0$ in an escape maneuver, f_v therefore approaches the impulsive limit. On the other hand, $a(\tau)$ decreases steadily during the backward integration of a capture maneuver so that as $v_j \to 0$, f_v approaches its low-thrust limit. For high values of v_j, $a(\tau)$ for both types of maneuvers is nearly constant, and the values of f_v approach a common asymptote.

From a physical viewpoint, however, the difference between escape and capture maneuvers is more apparent than real. When escapes and captures are compared on the basis of equal initial acceleration, the values of f_v are similar. This may be recalled from figures 5 to 7 and is further illustrated by the lower dashed and solid curves in figure 11.

---

[1] Recall that $\langle v \rangle$ is found by averaging v with respect to Δv_{ch}. Thus, in figure 10

$$\langle v \rangle_x = \frac{\text{area under curve } a - x}{\Delta v_{ch,x}}$$

In the low thrust limit, the $v - \Delta v_{ch}$ characteristic consists of straight line segments; then with $v_x = v_{\infty,x} = 0.5$, for instance,

$$\langle v \rangle_{\text{low thrust}} = \frac{0.5(1)(1) + 0.5(0.5)(1.50 - 1)}{1.50} = 0.417$$

Similarly,

$$\langle v \rangle_{\text{imp}} = 1 + \frac{\Delta v_{\text{imp}}}{2} = 1.25$$

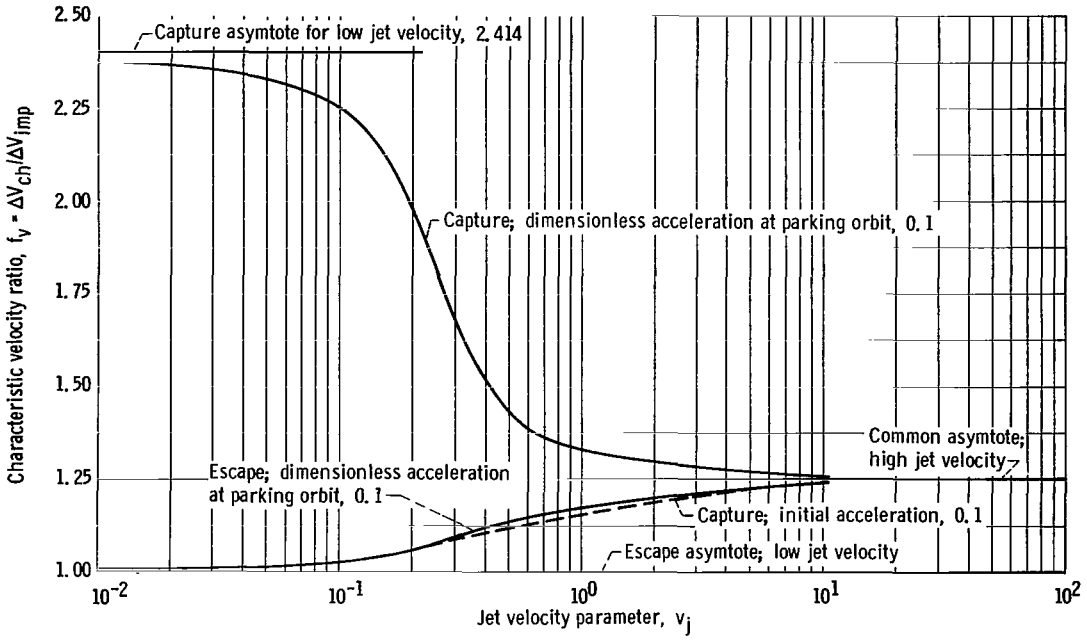

Figure 11. - Asymtotic comparison of escape and capture maneuvers. Hyperbolic velocity parameter, v_∞^2, 0.

Elliptic Orbits

Elliptic planetocentric parking orbits are of interest because they offer a significant reduction in propulsive ΔV for a given value of v_∞, as suggested by letting $e_{po} \to 1$ in equation (15). The reduction can approach 41.4 percent of $V_{c,ref}$; it is thus most significant for low periapse orbits about the major planets. At Jupiter, for instance, the saving can be as high as 10 miles per second, while at Mars it cannot exceed 0.8 mile per second.

Characteristic velocity ratios (f_v) and geometric data (ν_{po} and θ_{ch}) were presented in figure 3 for optimum-angle trajectories using an elliptic orbit with $e_{po} = 0.9$. This value of e_{po} was selected as a compromise between ΔV savings (cf eq. (15)) and orbital period considerations.

It may be seen in figure 3 that the f_v data for elliptic orbits are similar in appearance to those for circular orbits. The effects of v_∞^2, a_{po}, and v_j follow the same qualitative trends as in the circular orbit case. The two additional variables ν_{po} and e_{po} introduced by the consideration of elliptic orbits are now discussed.

Effects of initial true anomaly ν_{po}. - For the optimum-angle trajectories considered herein, the power-on or -off point on the ellipse ν_{po} is simply chosen in order to minimize f_v for given values of v_∞^2, a_{po}, and v_j. The characteristic angle θ_{ch} is regarded as a dependent variable; optimum values of θ_{ch} (i.e., corresponding to minimum

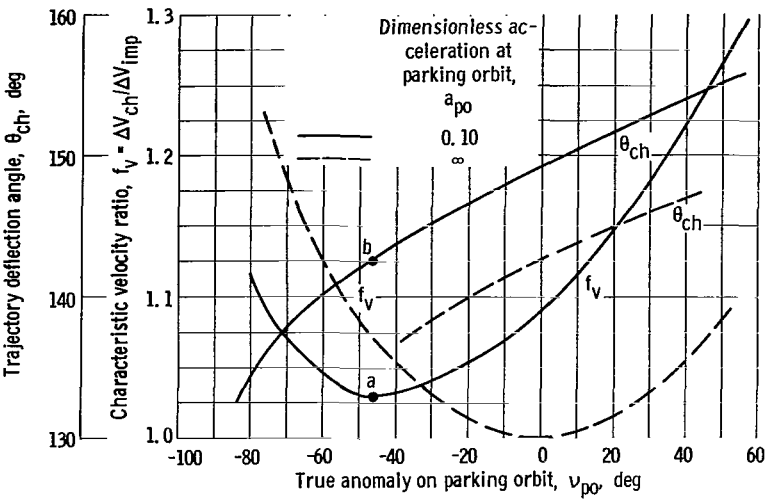

Figure 12. - Effect of true anomaly at elliptic parking orbit on escape or capture maneuver. Parking orbit eccentricity, 0.9; hyperbolic velocity parameter, 0.25; jet velocity parameter, ∞.

f_v) are presented. The process of selecting ν_{po} to minimize f_v is shown graphically in figure 12. The quantities f_v and θ_{ch} are plotted against ν_{po} for maneuvers where $e_{po} = 0.9$, $v_\infty^2 = 0.25$, and $v_j = \infty$. Impulsive and finite-thrust ($a_{po} = 0.1$) maneuvers are represented by the solid and dashed curves, respectively.

For the impulsive maneuver, the minimum value of $f_v = 1.0$ occurs at the periapse ($\nu_{po} = 0$); this choice obviously yields the maximum value of $\langle v \rangle$. The corresponding optimum value of θ_{ch} is 142°. The increase in f_v for nonoptimum angles represents the effect of a geometrical constraint alone on the propulsive efficiency and mean velocity.

For the maneuver with $a_{po} = 0.1$, the minimum value of $f_v = 1.03$ occurs at point a where $\nu_{po} = -47^\circ$. This choice maximizes $\langle v \rangle$ for equation (32) during the powered maneuver; it distributes the thrusting arc into roughly equal central angles ahead of and behind the original periapse. The associated optimum value of θ_{ch} (point b) is about 143°, only slightly different from the impulsive value (142°). It may be noted that θ_{ch} can be varied between 132° and 150° in this example for $f_v \leq 1.10$.

Effect of parking orbit eccentricity e_{po}. - While ν_{po} was selected in every case to yield minimum f_v, the choice of e_{po} is based primarily on mission objectives. Probably the highest value of e_{po} would be used which is compatible with the observations, experiments, and operations that constitute the purpose of the mission. Although the value of $e_{po} = 0.9$ is believed to be a good compromise, it is quite possible that lower or higher values may be required in particular cases.

The effect of other values of e_{po} is illustrated in figure 13 for the same maneuver ($v_\infty^2 = 0.25$, $a_{po} = 0.1$, $v_j = \infty$) as was discussed previously. The minimum values of f_v and the corresponding optimum values of ν_{po} and θ_{ch} are plotted against e_{po}. The

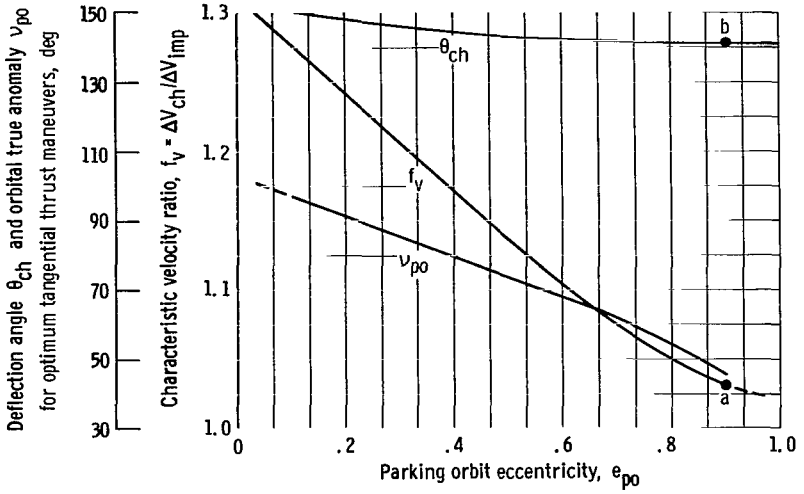

Figure 13. - Effect of parking orbit eccentricity on optimum tangential thrust maneuvers. Hyperbolic velocity parameter, 0.25; jet velocity parameter, ∞; dimensionless acceleration at parking orbit, 0.1; optimum orbital true anomaly chosen for minimum characteristic velocity ratio.

points a and b at $e_{po} = 0.9$ represent the values of f_v and θ_{ch} corresponding to the optimum ν_{po} as shown in figure 12.

It may be noted first that θ_{ch} varies little with e_{po}. More important is the fact that f_v decreases almost linearly with increasing e_{po}. Further examples (not illustrated here) indicate that this behavior is typical for maneuvers where $a_{po} \gtrsim 0.01$. Therefore, in this medium- to high-thrust regime, values of f_v for eccentricities between 0.0 and 0.9 can be estimated without major error from a linear formula such as

$$f_{v, e_{po}} = (1 - X) f_{v, 0.0} + X f_{v, 0.9}$$

where

$$X = \frac{e_{po}}{0.9}$$

Comparison of Elliptic and Circular Orbit Results

As was mentioned previously, the elliptic orbit data presented in figure 3 have the same general character as the circular orbit data of figure 2. There are, however, significant numerical differences. It was pointed out before that in the medium- to high-thrust regime ($a_{po} \gtrsim 0.01$) f_v tends to decrease with increasing e_{po}. The reason for

this may be understood by recalling that the optimization of ν_{po} amounted to placing as much of the maneuver as possible in a region of high velocity, that is, near the periapse. Hence, for short burn times (i.e., high accelerations and/or low velocity increments), $\langle v \rangle_{act} \approx \langle v \rangle_{imp}$. For elliptic orbits, the velocity increment and hence the burn time are lower than they are for a circle; therefore, a lower acceleration can be tolerated before f_v begins to increase sharply.

Very low-thrust systems, on the other hand, require such long burning times that only a relatively small part of the maneuver can be placed near the periapse. For the first few revolutions at least, the greater proportion of time will be spent in the vicinity of the apoapse, and this results in a low value of $\langle v \rangle$. Therefore, as predicted by equation (29) and shown in figure 3(a) (p. 30), the low-thrust values of f_v can become quite large as $e_{po} \to 1$. These high values cannot be reduced significantly by the use of variational steering control. They are therefore an inherent feature of the trajectories being considered and cannot be attributed to the assumed tangential steering law.

For these reasons it may be concluded that the ΔV savings predicted for elliptic parking orbits are actually enhanced by the finite-thrust effects if $a_{po} \gtrsim 0.01$, but they are degraded for very low-thrust systems. That is, the elliptic orbits are relatively more advantageous for high-thrust systems.

APPLICATION TO MISSION PROBLEMS

The foregoing discussion indicated the significance, interpretation, and use of the characteristic velocity correction factors (f_v) and geometric data that have been presented. This section will illustrate, by typical examples, the application of the data and procedures already described to actual mission problems.

Hohmann Transfers to All Planets

The minimum ΔV transfer between planets which lie in circular coplanar heliocentric orbits is the well-known Hohmann (180^o, contangential) trajectory. In view of equation (3), the Hohmann transfers will also yield low propellant fractions.

Table III lists the pertinent trajectory parameters for Hohmann transfers from the Earth to the other planets (except Pluto) of the solar system. The planets are assumed to lie in circular coplanar heliocentric orbits, and the transfers begin and end in circular planetocentric parking orbits at 1.1 planet radii. Representative values of I (900 sec) and A_i (0.2 $G_\oplus$) were assumed for the purpose of computing f_v. The circular parking orbits at 1.1 planet radii were chosen quite arbitrarily for the sake of comparison.

TABLE III. - IMPULSIVE VELOCITY CORRECTION FACTORS AND OTHER PROPERTIES FOR HOHMANN TRANSFERS FROM EARTH TO OTHER PLANETS

[Specific impulse, I, 900 sec; initial thrust to weight ratio, A_i, 0.2 $G_\oplus$.]

Parameter	Destination planet						
	Mercury ☿	Venus ♀	Mars ♂	Jupiter ♃	Saturn ♄	Uranus ♅	Neptune ♆
Departure from Earth							
Hyperbolic excess velocity at Earth departure, $V_{\infty,\oplus}$, miles/sec	4.66	1.56	1.85	5.46	6.38	7.02	7.26
Circular velocity at Earth parking orbit, $R_{po} = 1.1R_\oplus$	4.69	4.69	4.69	4.69	4.69	4.69	4.69
Gravity at Earth parking orbit, ft/sec^2	29.6	29.6	29.6	29.6	29.6	29.6	29.6
Impulsive velocity increment to depart Earth, $\Delta V_\oplus$, miles/sec	3.42	2.13	2.19	3.90	4.50	5.00	5.14
Hyperbolic velocity parameter, v_∞^2	0.987	0.111	0.155	1.351	1.850	2.239	2.391
Dimensionless acceleration at parking orbit, a_{po}	0.242	0.242	0.242	0.242	0.242	0.242	0.242
Jet velocity parameter, v_j	1.169	1.169	1.169	1.169	1.169	1.169	1.169
Characteristic velocity ratio, f_v	1.107	1.052	1.054	1.119	1.132	1.140	1.142
Arrival at planet							
Travel time (Earth to planet), days	106	146	259	1000	2200	5900	11 200
Hyperbolic excess velocity at planet arrival, $V_{\infty,pl}$, miles/sec	5.94	1.58	1.65	3.51	3.37	2.92	2.51
Circular velocity at planet parking orbit, $R_{po} = 1.1R_{pl}$	1.75	4.29	2.05	25.2	15.1	8.89	9.77
Gravity at planet parking orbit, ft/sec^2	9.6	22.9	10.65	70.2	31.2	24.2	27.4
Impulsive velocity increment to arrive at planet, ΔV_{pl}, miles/sec	4.69	1.94	1.29	0.45	6.40	3.95	4.28
Hyperbolic velocity parameter, v_∞^2	11.50	0.368	0.647	0.0194	0.0498	0.108	0.066
Dimensionless acceleration at parking orbit, a_{po}	1.585	0.406	0.769	0.69	0.706	0.562	0.532
Jet velocity parameter, v_j	3.130	1.277	2.673	0.218	0.363	0.616	0.561
Characteristic velocity ratio, f_v	<1.01	1.040	1.021	1.05 (extrapolated)	1.052	1.041	1.042

The hyperbolic excess velocity, the circular velocity, the local gravity, the impulsive velocity increments, the dimensionless parameters, and f_v are listed for both terminals of each Hohmann transfer. For Earth, Mars, and Venus, f_v was found from figures 5 to 7. For the capture maneuvers at the other planets, the previously described iterative procedure based on equation (10) was used with figure 2 to find a_{po}, v_∞^2, v_j, and thence f_v.

It is of some interest to note that with the chosen value of A_i ($0.2\ G_\oplus$) the correction factors at the destination planets are only slightly greater than unity (e.g., 1.05 at Jupiter). In fact, they are smaller than for the associated Earth escape maneuver. This somewhat surprising observation is the result of two effects which together determine a_{po}.

(a) For capture maneuvers, a_{po} is related to a_i by

$$a_{po} = \frac{a_i}{1 - m_p} = a_i e^{\Delta V_{ch}/G_\oplus I}$$

For the maneuvers under consideration, the mass ratio $e^{(\Delta V_{ch}/G_\oplus I)}$ ranges from about 2 (at Mars) to about 8 (at Jupiter). Thus A_{bo}, the acceleration at burnout, ranges from about 0.4 to 1.6 $G_\oplus$ since A_i was given as $0.2\ G_\oplus$.

(b) The a_{po} is then related to A_{bo} by equation (5c); that is,

$$a_{po} = \frac{A_{bo}}{G_{ref}}$$

The gravity ratio $G_\oplus/G_{ref}$ ranges from about 1 to 3 for all the planets except Jupiter, where it is about 0.4. For all planets, the net result is a fairly high value of a_{po} which, together with the generally low value of v_∞^2, leads to a low f_v.

Thus, for a one-way Hohmann trip to Jupiter, the neglect of finite-thrust effects leads to an error in ΔV_{ch} of 0.99 mile per second out of 14.35 miles per second, or about 7 percent.

Choosing the Circular Orbit Radius

The low circular parking orbits previously assumed were sufficient for a comparative discussion of the behavior of f_v at different planets. In an actual mission study, however, the choice of the parking orbit and the associated approach and departure maneuvers would receive very close attention. The low circular orbits have some definite

advantages, but it is also possible that more sophisticated orbits and maneuvers will be used in many cases. The purpose of this section, then, is to illustrate the use of the present data in finding an optimum parking orbit for a finite-thrust system.

The simplest approach to parking orbit optimization consists of just selecting the circular parking orbit radius $R_{po,opt}$ that will yield the lowest value of ΔV_{ch} for a given V_∞. Since the orbit is circular, the necessary hyperbolic direction for both the incoming and outgoing maneuvers (fig. 1(c), p. 6) can be attained with no ΔV penalty. Thus, the geometric effects are not considered in this example.

Inspection of equation (6) reveals that ΔV_{imp} is a function of the parking orbit radius alone for a circular orbit and given V_∞. It is readily seen that the minimum value of ΔV_{imp} occurs when

$$\left(\Delta V_{imp}\right)_{min} = V_{c,po} = \sqrt{\frac{\mu_{pl}}{R_{po,opt}}} = \frac{V_\infty}{\sqrt{2}} \tag{41}$$

or

$$R_{po,opt} = \frac{2\mu_{pl}}{V_\infty^2} \tag{42}$$

This is a well-known result for impulsive maneuvers. In the present case, however, it must be remembered that changing R_{po}, by changing $V_{c,ref}$ and G_{ref}, will affect the values of v_∞^2, a_{po}, and v_j. Thus, the changes of f_v as well as of ΔV_{imp} must be accounted for in seeking a minimum value of ΔV_{ch}.

As an example, consider the problem of selecting the optimum parking orbit radius for a representative Earth/Venus round trip, which has the characteristics listed in table IV. This trip has a total duration of 450 days of which 30 are to be spent in the Venus-centered parking orbit. Data were obtained from reference 1.

TABLE IV. - CHARACTERISTICS OF TYPICAL 450-DAY ROUND TRIP TO VENUS (1980)

Maneuver	Date (Julian)	Hyperbolic excess velocity, EMOS (miles/sec)
Earth departure	2444330	0.131 (2.43)
Venus arrival	2444450	.165 (3.05)
Venus departure	2444480	.164 (3.04)
Earth arrival	2444780	.298 (Atmospheric braking)

Since the Venus arrival and departure maneuvers involve about the same value of V_∞, it is sufficient to consider only one of them, for example, the departure for which $V_\infty = 3.04$ miles per second. Figure 14 shows f_v and ΔV_{ch} as functions of R_{po}/R_φ and A_i for this maneuver.

In the lower portion, f_v is shown for values of R_{po}/R_φ ranging from 1.1 to 16, I = 900 seconds, and initial thrust to weight ratios A_i of

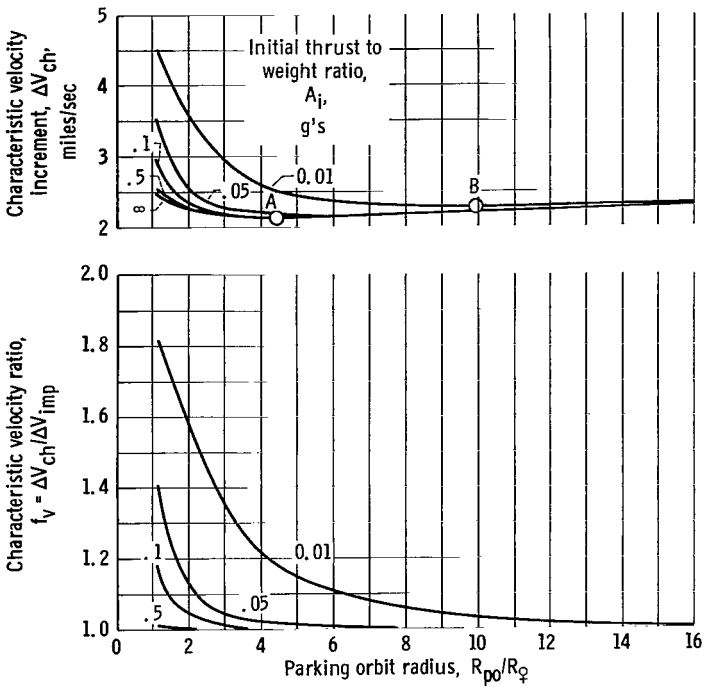

Figure 14. - Optimization of circular parking orbit radius for Venus escape maneuver. Hyperbolic velocity, 3.04 miles per second; specific impulse, 900 seconds.

∞, 0.5, 0.1, 0.05, and 0.01 $G_{\oplus}$. It may be noted that f_v falls off very rapidly as R_{po} increases; even for $A_i = 0.05\ G_{\oplus}$, f_v is inconsequential when R_{po} exceeds a few Venus radii. This, of course, is due to the fact that the term G_{ref} in the equation (5c) defining a_{po} (= A_{po}/G_{ref}) falls off as $1/R_{po}^2$; hence for a given value of A_i, a_{po} will become large at a sufficiently high radius.

The upper curve of figure 14 shows the values of $\Delta V_{ch} = f_v\, \Delta V_{imp}$ that result when the effects of R_{po} on both f_v and ΔV_{imp} are taken into account. The lower solid curve represents impulsive maneuvers ($A_i = \infty$); as predicted by equations (33) and (34), the minimum value of ΔV_{imp} (2.16 miles/sec) occurs where $R_{po}/R_{\varphi} = 4.4$. This radius is also nearly optimum for values of A_i as low as 0.1 $G_{\oplus}$; for smaller values, however, the optimum radius is higher. For instance if $A_i = 0.01\ G_{\oplus}$, then the minimum value of ΔV_{ch} (2.25 miles/sec) occurs at a radius $R_{po} \approx 10\ R_{\varphi}$. This is a lower characteristic velocity than the low orbit ($R_{po}/R_{\varphi} = 1.1$) impulsive value (2.48 miles/sec), yet the low value of A_i implies that a very small and light propulsion system could be used.

This example not only illustrates the effect of finite thrust on parking orbit selection, it also demonstrates a possible area of application for propulsion systems (such as arc jets) which might otherwise appear unattractive.

Optimization of Initial Thrust to Weight Ratio

Another frequently occurring mission problem that can be solved with the aid of the f_v data presented here is the selection of the optimum value of A_i. This is an important area of study, not only from the standpoint of minimizing the vehicle gross weight, but also because it has a direct bearing on the problem of selecting engine sizes for future development. For given values of V_{∞} and R_{po}, a high value of A_i implies a low value of m_p but a large, heavy engine: a low value of A_i implies a light engine but a high

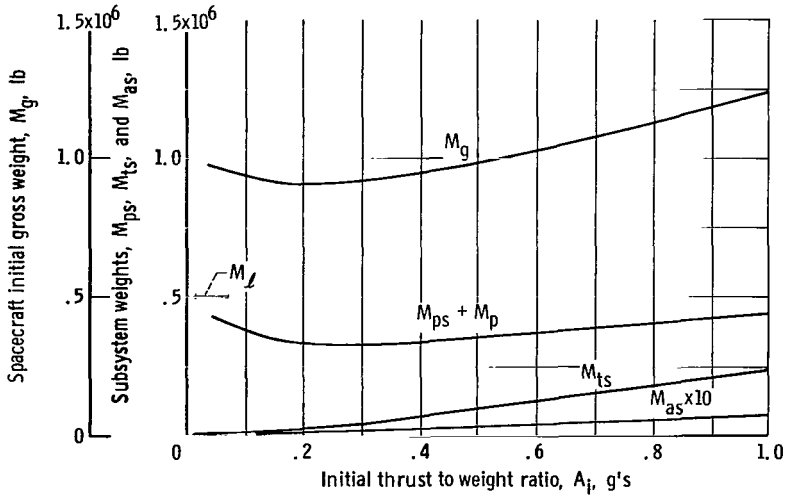

Figure 15. - Vehicle weights for typical Earth escape maneuver. Hyperbolic velocity, 2.43 miles per second; parking orbit radius, 1.1; specific impulse, 900 seconds; propellant sensitive structure fraction, 0.1; specific weight of engine and thrust structure, 0.2; acceleration sensitive structure fraction, 0.01.

propellant fraction. Thus, it may be anticipated that minimum M_g will occur for intermediate values of A_i, when there is a proper balance between propellant- and engine-related weights.

This process is illustrated by using the Earth-departure maneuver in table IV as a final example. In figure 15, the initial space vehicle gross mass in a low circular Earth parking orbit is plotted as a function of the initial acceleration. The propellant fractions are computed by using equation (3) and figure 5(a) (p. 42), with I = 900 seconds. Gross weights are then estimated from

$$M_g = M_\ell \frac{1 + A_{max} k_{as}}{(1 - m_p) - m_p k_{ps} - A_i k_{ts}} \tag{43}$$

where the following arbitrarily assumed parameter values were used:

Total Earth-departure payload, including upper stages:

$$M_\ell = 500\ 000 \text{ lb}$$

Propellant sensitive structure fraction:

$$k_{ps} = \frac{M_{ps}}{M_p} = 0.10$$

Specific weight of engine and thrust structure:

$$k_{ts} = \frac{M_{ts}}{F} = 0.20$$

Acceleration sensitive structure fraction:

$$k_{as} = \frac{M_{as}}{A_{max} M_{\ell}} = 0.01$$

The upper curve representing M_g has a minimum value of about 900 000 pounds when $A_i = 0.225\ G_{\oplus}$. The corresponding nuclear engine would have a thrust rating of about 200 000 pounds. The lower curves, which denote, respectively, the propellant and tankage weight, engine and thrust structure weight, and interstage structure weight, indicate how M_g is distributed among these major weight items.

CONCLUDING REMARKS

A wide range of data defining the essential dynamic and geometric characteristics (f_v and θ_{ch}) of continuous finite-thrust trajectories has been presented. These results are presented in dimensionless form and may be easily scaled to represent any case of physical interest. In this way, accurate propellant fractions and realistic trajectory geometry may be conveniently derived from impulsive interplanetary trajectory data.

The characteristic velocity ratio f_v is interpreted as a measure of the mean propulsive efficiency $\eta_{pr,m}$ along the powered arc. Both f_v and $\eta_{pr,m}$ are shown to be explicit functions of the mean tangential path velocity component $\langle v \cos u \rangle$. This quantity, and hence also f_v and $\eta_{pr,m}$, obviously are directly affected by the steering program $u(\tau)$ that is used, whether a significant gravity field is present or not. Thus, in the general case, f_v is as much due to steering losses as to gravity losses.

Of particular interest in this report is the class of optimum-angle trajectories. These are so named because both $u(\tau)$ and the initial power-on point are chosen only to minimize f_v (by maximizing $\langle v \cos u \rangle$) without regard to the consequent value of θ_{ch}. For such trajectories, it is shown in the appendix that tangential steering yields very nearly minimum values of f_v, especially in the case of an elliptic orbit.

These optimum-angle trajectories can always be used with circular parking orbits, because any final direction of $\vec{V}_{\infty}$ can be attained without penalty in f_v by merely selecting the appropriate power-on point. Optimum-angle trajectories can also be used for any

one maneuver based on an elliptic orbit by orienting the major axis at an angle θ_{ch} to $\vec{V}_{\infty}$. When two maneuvers are based on the ellipse, however (that is, during the capture - orbit-escape sequence at the destination planet of a round trip), it is generally necessary to reorient the ellipse (by means of auxiliary maneuvers) before optimum-angle trajectories can be used for both escape and capture. It remains to be seen whether or when the steering losses due to optimum constrained angle trajectories would result in a smaller overall penalty than the auxiliary orbit shifting maneuvers.

By its definition f_v is bounded above 1. An upper bound is also derived in the very low-thrust limit. This upper bound increases monotonically as e_{po} increases, ranging from 3.0 for a circular orbit to 10.6 for $e_{po} = 0.9$, and becomes very large as $e_{po} \to 1.0$. Thus for very low-thrust systems ($a_{po} \lesssim 0.001$), f_v is considerably larger for a maneuver from an elliptic orbit than it is for an equivalent circular orbit maneuver. This partially offsets the ΔV advantage of elliptic orbits. That is, the saving in the low-thrust ΔV_{ch} is smaller than the savings in ΔV_{imp}.

In direct contrast, medium- to high-thrust systems ($a_{po} \gtrsim 0.01$) have lower values of f_v for elliptic orbits than they do for equivalent maneuvers from a circular orbit. Therefore the advantage due to elliptic orbits is actually enhanced in this case (in the sense that the saving in characteristic velocity for finite thrust is greater than the saving in ΔV_{imp}).

Lewis Research Center,
National Aeronautics and Space Administration,
Cleveland, Ohio, April 12, 1966,
121-30-02-01-22.

APPENDIX - COMPARISON OF TANGENTIAL AND OPTIMUM STEERING CONTROL FOR ESCAPE FROM CIRCULAR AND ELLIPTIC PARKING ORBITS

Herein the tangential and optimal steering controls are compared for the problem of constant-thrust escape from circular and elliptic orbits. Previous work (reported in ref. 9) has shown that in the absence of geometric constraints, tangential steering is nearly optimal for constant acceleration departure maneuvers from a circular orbit to parabolic final energy ($v_\infty = 0$). These results are now extended to include maneuvers with $v_\infty \gtrless 0$, constant thrust, and elliptic parking orbits.

The Maximum Principle

The optimal angle-of-attack control program $u(\tau)$ is defined by Pontryagin's maximum principle (described in ref. 10). According to this, the control $u(\tau)$ can be optimal only if the function

$$\mathcal{H} = \psi_1 r' + \psi_2 v' + \psi_3 \alpha' + \psi_4 \theta' + \psi_5 \Delta v'_{ch} \tag{A1}$$

attains its maximum with respect to $u(\tau)$ for $0 \leq \tau \leq \tau_{bo}$. Furthermore, $\mathcal{H}$ is a constant, and its value is zero for an optimum-time trajectory. The state variable derivatives are given by equations (7) and (8), and the adjoint variables are defined by

$$\left.\begin{aligned}
\psi_1' &= -\frac{\partial \mathcal{H}}{\partial r} = -\left\{\frac{2 \sin \alpha}{r^3}\psi_2 + \left(\frac{2}{r^3 v} - \frac{v}{r^2}\right)\psi_3 \cos \alpha + \left(-\frac{v}{r^2}\cos \alpha\right)\psi_4\right\} \\
\psi_2' &= -\frac{\partial \mathcal{H}}{\partial v} = -\left\{\psi_1 \sin \alpha + \psi_3\left[-\frac{a_{po}}{1-m_p}\frac{\sin u}{v^2} + \left(\frac{1}{r} + \frac{1}{r^2 v^2}\right)\cos \alpha\right] + \frac{\psi_4 \cos \alpha}{r}\right\} \\
\psi_3' &= -\frac{\partial \mathcal{H}}{\partial \alpha} = -\left\{\psi_1 v \cos \alpha + \psi_2\left(-\frac{\cos \alpha}{r^2}\right) + \psi_3\left(\frac{v}{r} - \frac{1}{r^2 v}\right)(-\sin \alpha) + \psi_4 \frac{v}{r}(-\sin \alpha)\right\} \\
\psi_4' &= -\frac{\partial \mathcal{H}}{\partial \theta} = 0 \quad \text{or} \quad \psi_4 = \text{constant} \\
\psi_5' &= -\frac{\partial \mathcal{H}}{\partial \Delta v_{ch}} = 0 \quad \text{or} \quad \psi_5 = \text{constant}
\end{aligned}\right\} \tag{A2}$$

Since the range of $u(\tau)$ is not restricted, the maximum condition reduces to

$$\left.\begin{aligned} \frac{\partial \mathcal{H}}{\partial u} &= 0 \\ \frac{\partial^2 \mathcal{H}}{\partial u^2} &< 0 \end{aligned}\right\} \tag{A3}$$

and this leads to the optimal steering control law

$$\tan u(\tau) = \frac{\psi_3}{\psi_2 v} \tag{A4}$$

Transversality Conditions

Ten boundary conditions are required to specify the simultaneous solution of equations (A2) together with the equations of motion (7) and (8). For initial conditions are specified in terms of ν_{po} by equation (12), and one terminal condition is given in equation (13). Since the ψ's are homogeneous first-order functions, one of the initial values can be taken as a scale factor. The remaining four relations are defined by applying the transversality condition (ref. 10) at both the initial and final times.

At the initial time $\tau = 0$,

$$\sin \nu_{po} = \frac{1}{\psi_1 r^2 + \psi_2 / v} \left[\psi_3 r^2 \cos^2 \alpha \left(\frac{\cos \nu_{po} + e_{po}}{1 + e_{po}} \right) + \frac{1 + e_{po} \psi_4}{e_{po}} \right] \tag{A5}$$

This condition states that $\vec{\psi}_i$ is normal to the one-dimensional manifold defined by equation (12).

At the terminal time, the transversality condition yields the final three relations:

$$\psi_{3,bo} = \psi_{4,bo} = 0 \tag{A6}$$

$$\frac{\psi_{2,bo}}{\psi_{1,bo}} = r_{bo}^2 V_{bo} \tag{A7}$$

Solutions

The two-point boundary value nature of the problem requires an iterative solution to search in values of $\psi_i(0)$ that will lead, by means of equations of motion (7), the adjoint equations (A2), and the maximum condition (A4), to the desired terminal values (13), (A6), and (A7). Although five initial values of $\psi_i(0)$ are needed, all but two of these can be obtained without a numerical search.

(1) After $\psi_{1,i} - \psi_{4,i}$ have been selected, ψ_5 (a constant) is chosen so as to make $\mathcal{H} = 0$.

(2) In view of (A6) and (A2), $\psi_4 = 0$.

(3) Then, the initial value of ψ_1 is set equal to unity as the scale factor.

Thus, it only remains to find $\psi_{2,i}$ and $\psi_{3,i}$. For elliptic orbits, these may be found in terms of assumed values of u_i and ν_{po} by inverting equations (A4) and (A5):

$$\psi_{2,i} = \frac{\psi_{1,i} r_i^2 \sin \nu_{po} + \psi_4 \left(\dfrac{1 + e_{po}}{e_{po}} \right)}{\dfrac{\sin \nu_{po}}{v_i} - \left(r_i^2 \cos^2 \alpha_i \right) \left(\dfrac{\cos \nu_{po} + e_{po}}{1 + e_{po}} \right) v_i \tan u_i} \tag{A8}$$

$$\psi_{3,i} = \psi_{2,i} v_i \tan u_i \tag{A9}$$

Finally, the initial values u_i and ν_{po} are used as the independent variables in a two-dimensional search to satisfy the final conditions (13), (A6), and (A7). The use of these bounded, physically significant variables in place of the abstract ψ's results in a considerable practical simplification of the problem. The values of $u_i(0)$ and ν_{po} that correspond to an optimum tangential trajectory (figs. 3(s), (t), (u), and (v) and 4 to 8) provide excellent starting points for the search.

Conditions (A6) and (A7) have the further implication that for optimum-angle trajectories (where $\psi_4 = 0$) both $\psi_{3,bo}$ and its first derivative $\psi'_{3,bo}$ vanish at τ_{bo}. Thus, in view of equation (A4), the final portion of an optimum-angle trajectory is tangential to a high order. Any improvement due to optimal steering must therefore be generated in the early part of a trajectory. In the high-thrust limit, ψ'_3 remains bounded and therefore ψ_3 is continuous across an impulse. That is, tangential steering is the optimum control for impulsive thrust. Further, the transversality condition (A5) shows that this impulse is to be applied at periapse ($\nu_{po} = 0$) since $\psi_{3,i} = \psi_{4,i} = 0$.

TABLE V. - COMPARISON OF TANGENTIAL AND OPTIMAL ESCAPES FROM CIRCULAR ORBIT

[Dimensionless acceleration at parking orbit, a_{po}, 0.1.]

Hyperbolic velocity parameter, v_∞^2	Jet velocity parameter, v_j	Characteristic velocity ratio, f_v	
		Tangential escape	Optimal escape
0	∞	1.250	[a]1.241
0	1.0	1.179	1.171
.10	1.0	1.199	1.190
.25	1.0	1.225	1.214
.50	1.0	1.261	1.250
1.00	1.0	1.300	1.290

[a]From reference 9; all other values from present analysis.

Numerical Results

It is clear that tangential steering cannot satisfy the conditions of the maximum principle when finite thrust and nonzero burning times are considered. Nevertheless, there are two reasons to expect that tangential steering would yield nearly minimum Δv_{ch}:

(1) As pointed out before, at least the latter part of an optimal trajectory must be tangential to a high order.

(2) Tangential steering, as is well known, yields the maximum rate of increase of v_∞ at any instant. In table V, optimal- and tangential-thrust maneuvers are compared for escape from a circular orbit with $a_{po} = 0.1$. It is clear that in no case does optimal steering reduce f_v by more than 1 percent below the tangential value. Thus, the result of reference 9 is extended to the case of constant thrust as well as constant acceleration and to values of v_∞ in excess of zero (parabolic energy).

The effect of the eccentricity of an elliptic parking orbit is next illustrated in table VI. Here it is evident that, for the conditions chosen, the difference in f_v between tangential and optimal steering is greatest for circular orbits and decreases rapidly as

TABLE VI. - EFFECT OF PARKING ORBIT ECCENTRICITY ON CHARACTERISTIC VELOCITY RATIO FOR TANGENTIAL AND OPTIMAL STEERING

[Hyperbolic velocity parameter, v_∞^2, 0.1; dimensionless acceleration at parking orbit, a_{po}, 0.1; jet velocity parameter, ∞.]

Parking orbit eccentricity, e_{po}	Characteristic velocity ratio, f_v	
	Tangential steering	Optimal steering
0.9	1.011	1.011
.8	1.024	1.024
.6	1.066	1.065
.333	1.150	1.147
.00	1.270	1.260

TABLE VII. - EFFECT OF ORBIT ACCELERATION PARAMETER ON CHARACTERISTIC VELOCITY RATIO FOR TANGENTIAL AND OPTIMAL STEERING

[Parking orbit eccentricity, e_{po}, 0.9; hyperbolic velocity parameter, v_∞^2, 0.1; jet velocity parameter, ∞.]

Orbit acceleration parameter, a_{po}	Characteristic velocity ratio, f_v	
	Tangential steering	Optimal steering
0.1	1.011	1.011
.01	1.481	1.480
.001	4.261	4.256
.0001	6.890	6.871

e_{po} increases. That is, tangential steering is a better and better approximation to optimal as e_{po} increases.

Finally, in table VII, the effect of a_{po} on the comparison of tangential and optimum steering is illustrated for an elliptic orbit. From this it may be seen that, for all values of a_{po}, the difference in f_v for optimum as compared to tangential steering is a small fraction of 1 percent when an elliptic orbit is used. This is true even for very low accelerations for which f_v is large. Thus, the high values of f_v predicted (e.g., by eq. (29)) for elliptic orbit departures with low a_{po} and v_∞^2 are a true and inherent feature of the trajectories being considered; they are not due to any peculiarity of the tangential steering law.

In summary, it may be inferred from the foregoing discussion that across-the-board incorporation of optimal steering control would not modify the conclusions nor significantly change the data presented in the body of this report.

REFERENCES

1. Anon: Planetary Flight Handbook. Vol. 3 of Space Flight Handbooks. NASA SP-35, parts 1-3, 1963.

2. Knip, Gerald, Jr.; and Zola, Charles L.: Three-Dimensional Trajectory Analysis for Round-Trip Missions to Mars. NASA TN D-1316, 1962.

3. Willis, Edward A., Jr.: Optimization of Double-Conic Interplanetary Trajectories. NASA TN D-3184, 1966.

4. Benney, J. D.: Escape from a Circular Orbit Using Tangential Thrust. Jet Propulsion, vol. 28, no. 3, Mar. 1958, pp. 167-169.

5. Petraits, John J.: Correction Factor for Initial Acceleration Effects on Impulsive Mission Requirements. ARS J, vol. 32, no. 6, June 1962, pp. 957-959.

6. Moeckel, W. E.: Trajectories with Constant Tangential Thrust in Central Gravitational Fields. NASA TR R-53, 1960.

7. Luidens, Roger W.; and Miller, Brent A.: Efficient Planetary Parking Orbits with Examples for Mars. NASA TN D-3220, 1966.

8. Lawden, Derek F.: Impulsive Transfer Between Elliptical Orbits. Optimization Techniques with Applications to Aerospace Systems, George Leitmann, ed., Academic Press, 1962, pp. 323-351.

9. Lebedev, V. N.: Variational Problem of Escape from Circular Orbit. Rep. No. FTD-TT-64-1200/1+1+2+4, Foreign Technology Div., Air Force Systems Command, Dec. 1964. (Available from DDC as AD-610208).

10. Pontryagin, L. S.; Boltyanskii, V. G.; Gamkrelidze, R. V.; and Mishchenko, E. F. (Konstantin Trirogoff, trans.): The Mathematical Theory of Optimal Processes. Lucien Neustadt, trans. ed., Interscience Publishers, 1962.

"The aeronautical and space activities of the United States shall be conducted so as to contribute . . . to the expansion of human knowledge of phenomena in the atmosphere and space. The Administration shall provide for the widest practicable and appropriate dissemination of information concerning its activities and the results thereof."

—NATIONAL AERONAUTICS AND SPACE ACT OF 1958

NASA SCIENTIFIC AND TECHNICAL PUBLICATIONS

TECHNICAL REPORTS: Scientific and technical information considered important, complete, and a lasting contribution to existing knowledge.

TECHNICAL NOTES: Information less broad in scope but nevertheless of importance as a contribution to existing knowledge.

TECHNICAL MEMORANDUMS: Information receiving limited distribution because of preliminary data, security classification, or other reasons.

CONTRACTOR REPORTS: Technical information generated in connection with a NASA contract or grant and released under NASA auspices.

TECHNICAL TRANSLATIONS: Information published in a foreign language considered to merit NASA distribution in English.

TECHNICAL REPRINTS: Information derived from NASA activities and initially published in the form of journal articles.

SPECIAL PUBLICATIONS: Information derived from or of value to NASA activities but not necessarily reporting the results of individual NASA-programmed scientific efforts. Publications include conference proceedings, monographs, data compilations, handbooks, sourcebooks, and special bibliographies.

Details on the availability of these publications may be obtained from:

SCIENTIFIC AND TECHNICAL INFORMATION DIVISION

NATIONAL AERONAUTICS AND SPACE ADMINISTRATION

Washington, D.C. 20546